Electromagnetic unidirectionality in magnetic photonic crystals

A. Figotin and I. Vitebskiy
Department of Mathematics, University of California at Irvine, California 92697
(Received 22 August 2002; revised manuscript received 22 November 2002; published 28 April 2003)

We study the effect of electromagnetic *unidirectionality*, which can occur in magnetic photonic crystals under certain conditions. A unidirectional periodic medium, being perfectly transparent for an electromagnetic wave of certain frequency, ''freezes'' the radiation of the same frequency propagating in the opposite direction. One of the most remarkable manifestations of the unidirectionality is that while the incident radiation can enter the unidirectional slab in either direction with little or even no reflectance, it cannot escape from there getting trapped inside the periodic medium in the form of the coherent frozen mode. Having entered the slab, the wave slows down dramatically and its amplitude increases enormously, creating unique conditions for nonlinear phenomena. Such a behavior is an extreme manifestation of the spectral nonreciprocity, which can only occur in gyrotropic photonic crystals. Unidirectional photonic crystals can be made of common ferro- or ferrimagnetic materials alternated with anisotropic dielectric components. A key requirement for the property of unidirectionality is the proper spatial arrangement of the constitutive components.

DOI: 10.1103/PhysRevB.67.165210 PACS number(s): 78.20.Bh, 41.20.Jb, 78.20.Ls, 42.65.−k

I. INTRODUCTION

A. Unidirectional photonic crystals

Photonic crystals are spatially periodic composites made up of lossless dielectric components. As a consequence of spatial periodicity, the electromagnetic frequency spectrum of a photonic crystal develops a band-gap structure similar to that of electrons in semiconductors and metals (see, for instance, Refs. 1–6 and references therein). Gyrotropic photonic crystals are those in which at least one of the constitutive components is a magnetic material (a ferromagnet or a ferrite) displaying the Faraday rotation.[7–9] Such materials are often referred to as gyrotropic or bigyrotropic. If a gyrotropic photonic crystal satisfies certain symmetry conditions formulated in Ref. 10, its bulk electromagnetic dispersion relation $\omega(\vec{k})$ may display asymmetry with respect to the Bloch wave vector $\vec{k}$,

$$\omega(\vec{k}) \neq \omega(-\vec{k}), \tag{1}$$

as shown in Fig. 1.

The bulk spectral asymmetry (1) by no means occurs automatically in any magnetic photonic crystal. Quite the opposite, only special periodic arrays of magnetic and other dielectric components can produce the effect.[25] An example of a such periodic stack is shown in Fig. 2. The degree of the spectral asymmetry depends on the magnitude of circular birefringence of the gyrotropic component, as well as on some other geometric and physical parameters of the periodic array. Detailed theoretical analysis of the problem along with a number of specific examples are provided in Ref. 10.

The property of bulk spectral asymmetry has various physical consequences, one of which is the effect of *unidirectional wave propagation*. Let us consider a transverse monochromatic wave propagating along a symmetry direction z of a gyrotropic photonic crystal. The Bloch wave vector $\vec{k}$, as well as the group velocity $\vec{u}(\vec{k}) = \partial\omega(\vec{k})/\partial\vec{k}$ are parallel to z. Let us denote

$$k = k_z, \quad u(k) = \partial\omega(k)/\partial k, \tag{2}$$

and suppose that one of the spectral branches $\omega(k)$ has a stationary inflection point at $k = k_0$, $\omega = \omega_0$,

$$\left.\frac{\partial\omega}{\partial k}\right|_{k=k_0} = 0; \ \left.\frac{\partial^2\omega}{\partial k^2}\right|_{k=k_0} = 0; \ \left.\frac{\partial^3\omega}{\partial k^3}\right|_{k=k_0} \neq 0, \tag{3}$$

as shown in Fig. 1. Note that there are two propagating (extended) Bloch waves with frequency $\omega = \omega_0$: one with $k = k_0$, and the other with $k = k_1$. Obviously, only one of the two waves can transfer electromagnetic energy—the one with $k = k_1$ and the group velocity $u(k_1) < 0$. The Bloch eigenmode with $k = k_0$ has zero group velocity $u(k_0) = 0$ and does not transfer energy. This latter eigenmode associated with stationary inflection point (3) is referred to as the *frozen mode*. As one can see in Fig. 1, none of the eigenmodes with $\omega = \omega_0$ has positive group velocity and therefore none of the electromagnetic eigenmodes can transfer the energy from left to right at this particular frequency! Thus a photonic crystal with the dispersion relation similar to that in Fig. 1 displays the property of *electromagnetic unidirectionality* at $\omega = \omega_0$. Such a remarkable effect can be viewed as an extreme manifestation of the spectral asymmetry (1).

According to Ref. 10, the effect of unidirectionality can occur in magnetic photonic crystals made up of common dielectric and ferro- or ferrimagnetic components (at least at frequencies below 10^{12}Hz). There are two key physical requirements for that:

(i) The space arrangement of the constitutive components must satisfy certain symmetry criterion for spectral asymmetry. This criterion, specified in Ref. 10, rules out all nonmagnetic and the majority of magnetic photonic crystals. The space arrangement of magnetic and other constitutive components must be complex enough to allow for the bulk spectral asymmetry (1).

(ii) The magnetic constituent (for instance, ferrite) must display significant circular birefringence at frequency range of interest, for example, several percent or more. Failure to

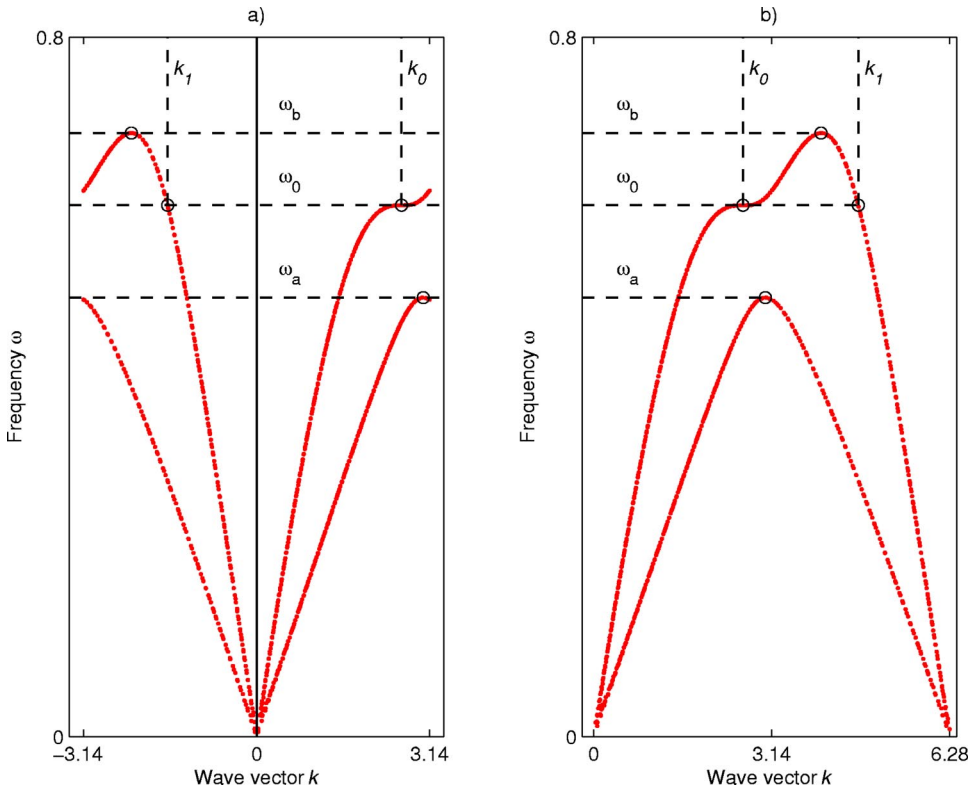

FIG. 1. An example of asymmetric bulk electromagnetic dispersion relation of a periodic magnetic stack. At $\omega=\omega_0$, $k=k_0$, one of the spectral branches develops a stationary inflection point (3) associated with the frozen mode. ω_b is the edge of the lowest frequency band. The graphs (a) and (b) represent two different choices of the Brillouin zone. The values ω and k are expressed in units of c/L and $1/L$, respectively.

satisfy this condition does not formally rule out the phenomenon of unidirectionality, but it makes the magnitude of the effect insignificant. Indeed, weak Faraday rotation leads to a small value of the third derivative $(\partial^3\omega/\partial k^3)_{k=k_0}$ in Eq. (3), which, in turn, pushes the stationary inflection point ω_0 in Fig. 1 too close to the photonic band edge ω_b.

The simplest and, perhaps, the most practical periodic structures displaying the property of unidirectionality are one-dimensional (1D) periodic magnetic stacks, an example of which is presented in Fig. 2. If the above two conditions

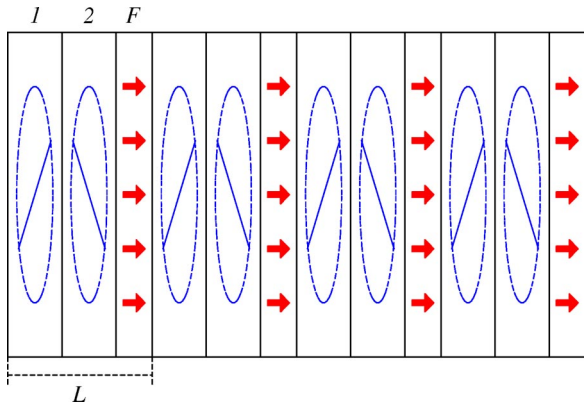

FIG. 2. A simplest periodic magnetic stack supporting asymmetric bulk dispersion relation. Each primitive cell $L=2A+F$ comprises three layers: two anisotropic dielectric layers 1 and 2 of thickness A and with misaligned in-plain anisotropy, and one magnetic layer of thickness F and magnetization shown by the arrows. The misalignment angle between adjacent layers 1 and 2 must be different from 0 and $\pi/2$.

are met, one can always achieve electromagnetic unidirectionality at a given frequency ω_0 by adjusting at least two different physical and/or geometrical parameters, such as

- the ratio $\rho=F/A$ of the layers thicknesses,
- the misalignment angle $\varphi=\varphi_1-\varphi_2$ between anisotropic dielectric layers,
- magnetic permeability and/or electric permittivity of the layers (this can be done by application of external homogeneous magnetic or electric field[19,20]).

Physical manifestations of the electromagnetic unidirectionality prove to be rather universal and dependent solely on the dispersion relation $\omega(\vec{k})$ in the vicinity of the frozen mode frequency ω_0. An essential characteristic determining the magnitude of the respective electromagnetic abnormalities is the dimensionless parameter

$$\phi=\frac{1}{\omega_0 L^3}\left(\frac{\partial^3\omega}{\partial k^3}\right)_{k=k_0}, \tag{4}$$

where L is the length of the primitive cell of the photonic crystal. For instance, periodic stacks made of different constitutive materials and having completely different geometry, display, nevertheless, very similar behavior in the vicinity of the frozen mode frequency, provided that they have comparable values of the parameter ϕ from Eq. (4). For this reason, all numerical examples considered in this paper are based on a single magnetic periodic stack shown in Fig. 2 and described in detail in Appendix A. These examples illustrate the universal features of electromagnetic behavior of all unidirectional photonic crystals.

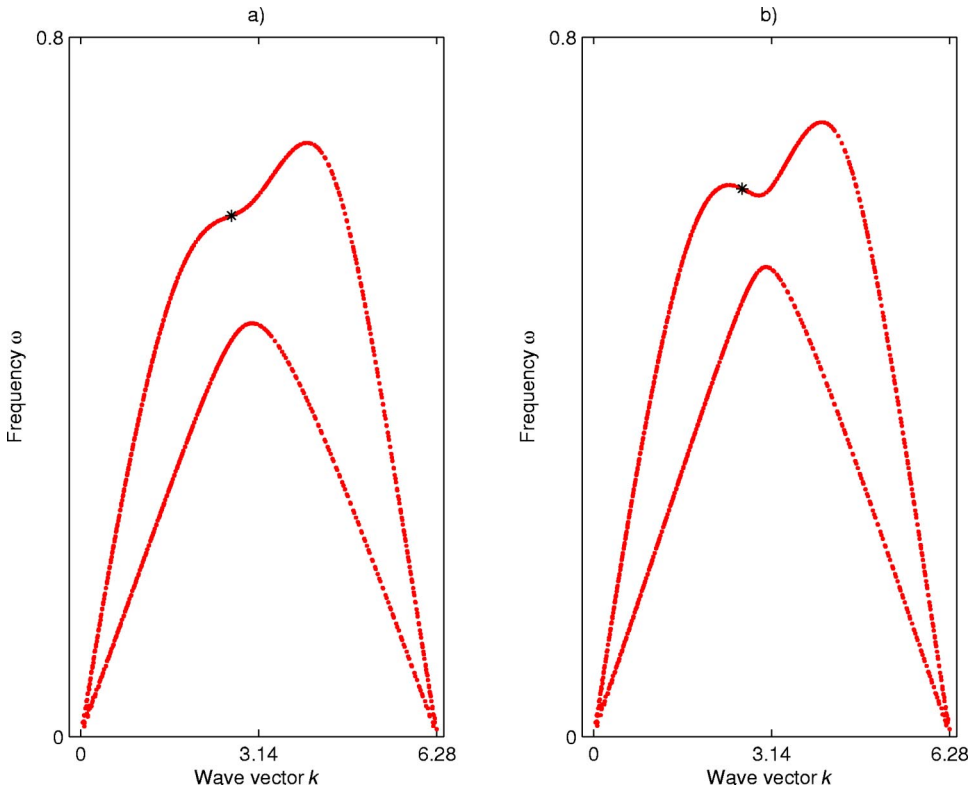

FIG. 3. Asymmetric dispersion relations of the periodic structures slightly modified compared to that related to Fig. 1. In both cases, the stationary inflection point of Fig. 1 evolves into a simple inflection point with $\omega''_{kk}(k) \neq 0$: (a) the ratio $\rho = F/A$ of the layers thicknesses exceeds the the critical value ρ_0 by a third; (b) $\rho < \rho_0$ by a third. Here ρ_0 is the "unidirectional" ratio corresponding to the situation in Fig. 1.

If any of the physical or geometrical parameters of a unidirectional stack is altered, the stationary inflection point (3) can turn into a regular inflection point corresponding to a finite group velocity, as shown in Fig. 3(a), or a pair of close inflection points, as in the situation in Fig. 3(b). This blurs and weakens the effects associated with electromagnetic unidirectionality.

At first sight, the existence of the frozen mode related to a stationary inflection point (3) does not require the spectral asymmetry (1). Indeed, a hypothetical symmetric dispersion relation in Fig. 4(a) would have a pair of stationary inflection points, although there would be no spectral asymmetry, let alone unidirectionality, in such a case. But in fact, the situation similar to that in Fig. 4(a) cannot occur regardless of the complexity of the composite structure. At any given frequency, there cannot be more than one stationary inflection point (3) in the electromagnetic spectrum. Therefore *the frozen mode cannot exist in periodic stacks, either magnetic or nonmagnetic, with symmetric dispersion relations* $\omega(\vec{k}) = \omega(-\vec{k})$.

On the other hand, whenever the electromagnetic dispersion relation has a stationary inflection point (3) (i.e., the frozen mode), it always displays the property of unidirectionality at the same frequency. This implies that a hypothetical dispersion relation in Fig. 4(b) having a stationary inflection point at $\omega = \omega_0$ but not displaying electromagnetic unidirectionality at the respective frequency, cannot occur either. Recall that the unidirectionality means the existence of propagating modes with only negative (or only positive) group velocity at a given frequency and given direction of propagation.

The above statements suggest a strict one-to-one correspondence between the existence of the frozen mode and the property of unidirectionality at the same frequency in peri-

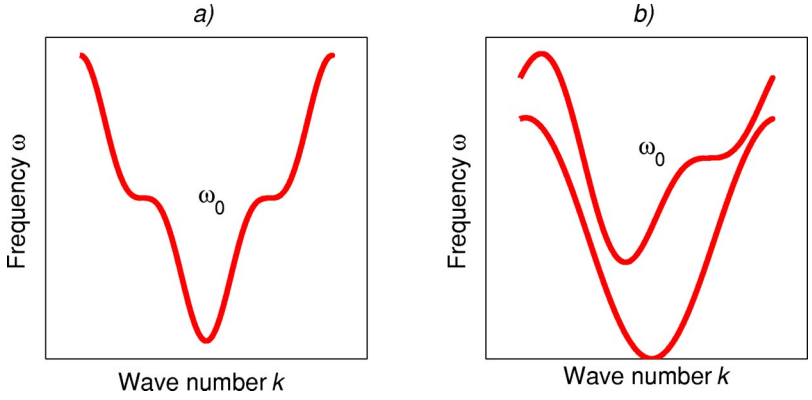

FIG. 4. Hypothetical dispersion relations, which cannot exist in any periodic stack regardless of its complexity: (a) symmetric dispersion relation with two stationary inflection points at the same frequency ω_0; (b) asymmetric dispersion relation with stationary inflection point (the frozen mode) at $\omega = \omega_0$, but without the property of unidirectionality at the same frequency.

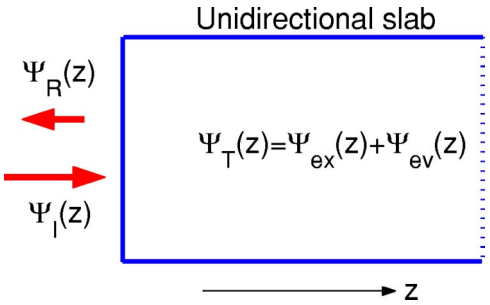

FIG. 5. Forward (left-to-right) normal incidence on the surface of a semi-infinite unidirectional slab with the dispersion relation in Fig. 1; the frequency ω lies within the range $\omega_a<\omega<\omega_b$. $\Psi_I(z)$ and $\Psi_R(z)$ are the incident and reflected waves in vacuum; $\Psi_{ex}(z)$ and $\Psi_{ev}(z)$ are the extended (with $u>0$) and the evanescent (with $\mathrm{Im}\,k>0$) contributions to the transmitted wave $\Psi_T(z)$.

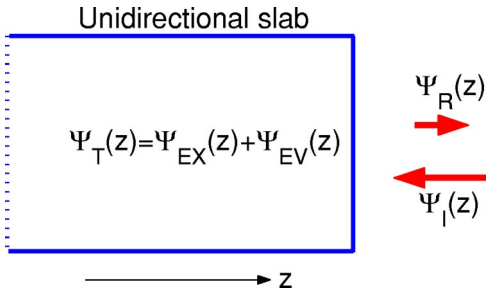

FIG. 6. Backward (right-to-left) normal incidence on the surface of a semi-infinite unidirectional slab with the dispersion relation in Fig. 1; the frequency ω lies within the range $\omega_a<\omega<\omega_b$. $\Psi_I(z)$ and $\Psi_R(z)$ are the incident and reflected waves in vacuum; $\Psi_{EX}(z)$ and $\Psi_{EV}(z)$ are the extended (with $u<0$) and the evanescent (with $\mathrm{Im}\,k<0$) contributions to the transmitted wave $\Psi_T(z)$.

odic layered media. This is a consequence of the fact that the dispersion relation $\omega(k)$ of a periodic stack is determined by characteristic equation of the fourth degree. Indeed, at a given frequency ω, there must be a total of four real and complex solutions for the wave vector $\vec{k}\|z$. Taking into consideration that a stationary inflection point (3) is always associated with a triple real root of the characteristic equation, one can come to the following conclusions:

(i) There cannot be more than one frozen mode at the same frequency ω_0. For instance, the dispersion relation in Fig. 4(a) showing a couple of inflection points at the same frequency cannot occur.

(ii) There must be one and only one additional eigenmode at the frequency ω_0 of the frozen mode with the wave vector k different from k_0. For instance, the dispersion relation in Fig. 4(b) showing three additional eigenmodes at the frequency of the frozen mode, cannot occur either.

Detailed consideration of the bulk electromagnetic spectra in infinite periodic gyrotropic stacks is presented in Sec. II, where we thoroughly analyze a peculiar behavior of the extended and evanescent modes in nonreciprocal periodic stacks. Emphasis is given to the vicinity of stationary inflection point where the phenomenon of unidirectionality occurs. Importantly, if the frequency ω exactly coincides with ω_0 from Eq. (3), the electromagnetic field inside the unidirectional periodic array does not reduce to a linear superposition of canonical Bloch eigenmodes. The latter peculiarity is related to the triple degeneracy of the stationary inflection point. The results of Sec. II are further applied to semi-infinite and finite unidirectional slabs.

B. Electromagnetic properties of a semi-infinite unidirectional slab

The phenomenon of unidirectionality is associated with unique electromagnetic properties of periodic media in the vicinity of the frozen mode frequency ω_0. Some preliminary conclusions can be drawn from the energy conservation consideration. Consider a plane electromagnetic wave impinging on the surface of a semi-infinite unidirectional photonic crystal, as shown in Fig. 5. The direction z of wave propagation is perpendicular to the photonic slab boundary and coincides with the z axis in Eqs. (2) and (3). Due to the spectral asymmetry of the slab, the situation of the reversed incidence presented in Fig. 6 appears to be quite different and will be considered later on.

Let $S_I>0$, $S_R\leqslant 0$ and $S_T\geqslant 0$ be the energy flux of the incident (Ψ_I), reflected (Ψ_R) and transmitted (Ψ_T) waves, respectively. The energy conservation yields

$$S_I+S_R=S_T \tag{5}$$

or, equivalently

$$S_T=\tau S_I, \quad S_R=-\rho S_I, \quad \rho=1-\tau, \tag{6}$$

where τ and ρ are the normal transmittance and reflectance of the semi-infinite slab, respectively ($0\leqslant\tau\leqslant 1, 0\leqslant\rho\leqslant 1$). Assume that the wave frequency ω lies within the frequency range

$$\omega_a<\omega<\omega_b \tag{7}$$

in Fig. 1. In such a case, the transmitted wave $\Psi_T(z)$ inside the slab is a superposition of one extended (propagating) Bloch eigenmode $\Psi_{ex}(z)$ (the one with $u>0$) and one evanescent mode $\Psi_{ev}(z)$ (the one with $\mathrm{Im}\,k>0$), as shown in Fig. 5. Evanescent eigenmodes, which are not shown in the dispersion relation in Fig. 1, do not contribute to the energy flux, therefore the extended eigenmode $\Psi_{ex}(z)$ is the only one contributing to the energy flux S_T transmitted inside the slab. In the case of a single propagating mode, the energy flux S_T can be expressed in terms of the mode energy density W_{ex} and its group velocity u from Eq. (2)

$$S_T=uW_{ex}. \tag{8}$$

The fact that the group velocity u vanishes as $\omega\to\omega_0$, implies two possible scenarios, depending on whether the energy flux S_T inside the slab also vanishes as $\omega\to\omega_0$.

The most obvious scenario would be

$$S_T\to 0, \tau\to 0, \quad \text{as } \omega\to\omega_0, \tag{9}$$

which implies a total reflectance of the incident wave at $\omega=\omega_0$. Such a behavior would be similar to what commonly occurs in any semi-infinite photonic slab in the vicinity of a

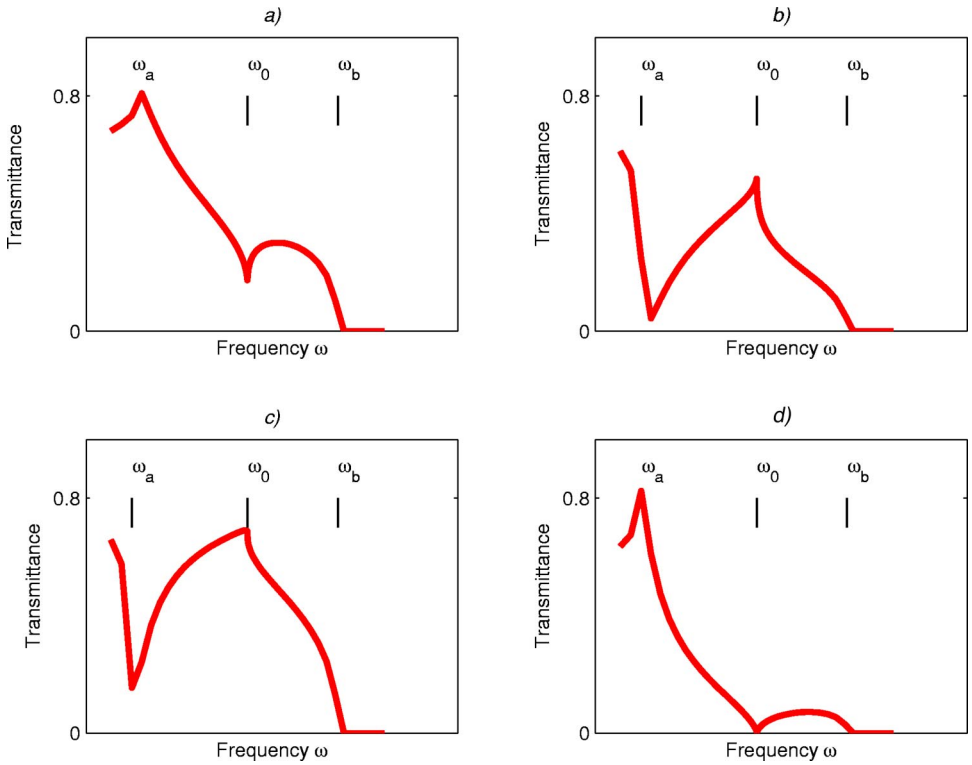

FIG. 7. Transmittance τ_e of semi-infinite unidirectional slab vs frequency ω (in units of c/L) for the case of forward incidence shown in Fig. 5. The characteristic frequencies are explained in Fig. 1. The incident wave polarization is: (a) linear, with $\vec{E}\|x$; (b) linear, with $\vec{E}\|y$; (c) elliptic, corresponding to maximal transmittance at $\omega=\omega_0$; (d) elliptic, that produces a single extended mode $\Psi_{ex}(z)$ inside the slab (no evanescent mode contribution).

photonic band edge, where the group velocity of the extended eigenmode also vanishes. Specifically, referring to the example in Fig. 1, we have in the vicinity of the photonic band edge at $\omega=\omega_b$

$$S_T\to 0,\quad \tau\to 0,\quad \text{as}\quad \omega\to\omega_b \tag{10}$$

as illustrated in Fig. 7. This common situation occurs in any semi-infinite photonic crystal near photonic band edges.

By contrast, it turns out that in the vicinity of the frozen mode frequency ω_0 we have, instead of Eq. (9),

$$S_T\to S_0>0,\quad \tau\to\tau_0>0,\quad W_T\to\infty,\quad \text{as}\quad \omega\to\omega_0. \tag{11}$$

In such a case, the incident wave Ψ_I with the frequency ω close to ω_0 can enter the semi-infinite unidirectional slab with little or even no reflectance [see Figs. 7(a),(c) where the transmittance τ remains finite in the vicinity of ω_0]. Having entered the slab, the incident wave converts into nearly frozen extended mode $\Psi_{ex}(z)$ and slows down dramatically. Immediately upon entering the slab, the wave amplitude $|\Psi_T(z)|^2$ is limited, as shown in Fig. 8(a), but then it gradually increases until reaches its saturation value

$$|\Psi_{ex}(z)|^2\sim|\omega-\omega_0|^{-2/3}. \tag{12}$$

The distance l from the slab boundary, at which the wave intensity approaches its maximum value (12), is also strongly dependent on $|\omega-\omega_0|$,

$$l\sim\left|\left(\frac{\partial^3\omega}{\partial k^3}\right)_{k=k_0}(\omega-\omega_0)^{-1}\right|^{1/3}. \tag{13}$$

Relatively small amplitude of the electromagnetic field $\Psi_T(z)$ in the transient region $z\ll l$ is due to a destructive interference of the nearly frozen mode $\Psi_{ex}(z)$ and the evanescent mode $\Psi_{ev}(z)$ with $\mathrm{Re}\,k>0$. As illustrated in Figs. 8 and 9(a) and (b), both contributions have huge and nearly equal and opposite values near the slab boundary, so that their superposition $\Psi_T(0)=\Phi_T=\Phi_{ex}+\Phi_{ev}$ at $z=0$ is relatively small, as shown in Fig. 9(c). The destructive interference allows to satisfy the boundary condition (81) at the semi-infinite slab boundary. At $z\gg l$ the contribution of the

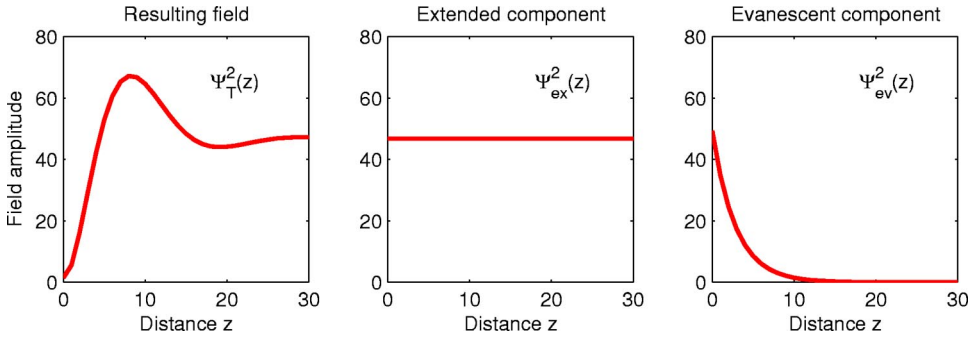

FIG. 8. Amplitude of the resulting electromagnetic field $\Psi_T(z)$ and its extended and evanescent components $\Psi_{ex}(z)$ and $\Psi_{ev}(z)$ inside unidirectional slab. z is the distance from the slab surface in units of L. Frequency ω is close to ω_0 (specifically, $\omega-\omega_0=0.05\omega_0$). The amplitude $|\Psi_I|^2$ of the incident radiation is equal to unity.

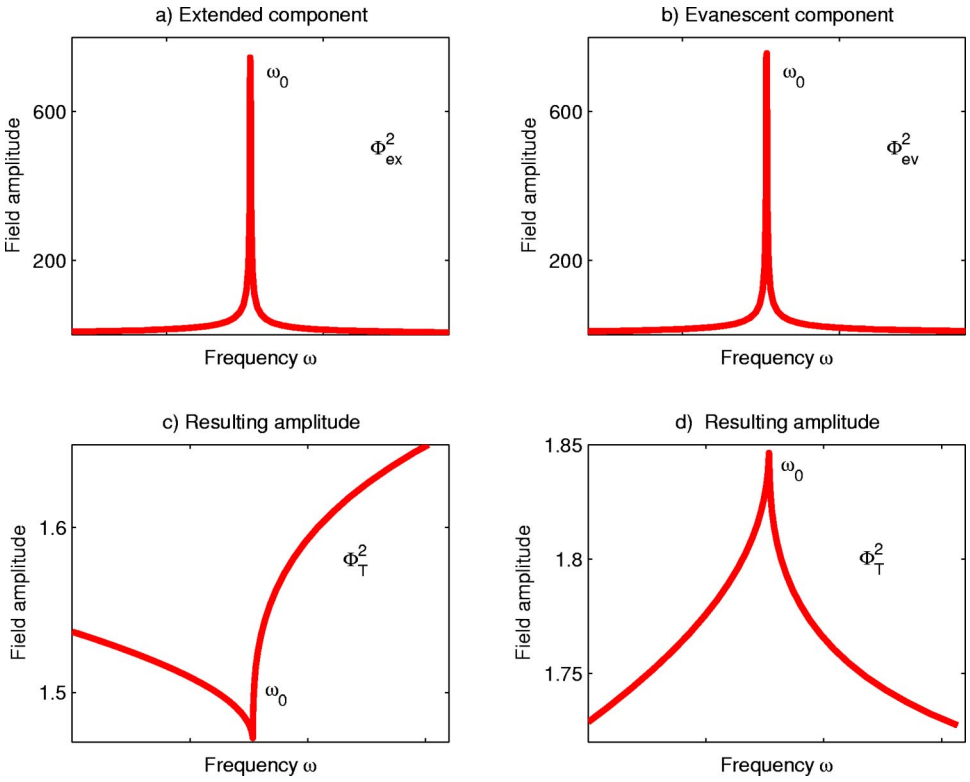

FIG. 9. Destructive interference of the extended and the evanescent components of electromagnetic field $\Phi_T=\Psi_T(0)$ at the surface of semi-infinite unidirectional slab for the case of forward incidence: (a) extended (nearly frozen) contribution $|\Phi_{ex}|^2=|\Psi_{ex}(0)|^2$ for $\vec{E}\|y$; (b) evanescent contribution $|\Phi_{ex}|^2=|\Psi_{ex}(0)|^2$ for $\vec{E}\|y$; (c) the resulting field amplitude $|\Phi_T|^2=|\Phi_{ex}+\Phi_{ev}|^2$ for $\vec{E}\|y$; (d) the resulting field amplitude for $\vec{E}\|x$.

evanescent mode $\Psi_{ev}(z)$ decays exponentially, while the contribution of the extended mode $\Psi_{ex}(z)$ remains constant and huge. As a result, the total electromagnetic field amplitude $\Psi_T(z)$ inside the slab gradually increases with the distance z until reaches its maximum value of $\Psi_{ex}(z)$ from Eq. (12), as illustrated in Fig. 8(a). If the frequency ω exactly coincides with ω_0, the transmitted wave $\Psi_T(z)$ inside the unidirectional slab is not a superposition of canonical Bloch eigenmodes, and its amplitude inside the slab diverges

$$\text{at} \quad \omega=\omega_0: \quad |\Psi_T(z)|^2\sim z^2, \quad \text{as} \quad z\to\infty \qquad (14)$$

as shown in Fig. 10.

The phenomenon described by formulas (12) and (14) and illustrated in Figs. 8 and 10 can be viewed as *unidirectional freezing* of the incident electromagnetic wave inside the semi-infinite unidirectional slab. It is accompanied by a dramatic slowdown of the transmitted wave inside the slab, as well as a huge increase in its amplitude. *Remarkably, the transmittance τ_e of the semi-infinite slab remains finite and can be even close to 100%*. By contrast, in the situation when the plane electromagnetic wave of the same frequency ω close or equal to ω_0 impinges on the surface of the same unidirectional stack but from the opposite direction, as shown in Fig. 6, nothing extraordinary occurs. The incident wave gets partially reflected, and the rest continues inside the slab in the form of the extended Bloch eigenmode $\Psi_{EX}(z)$ with finite group velocity $u(k_1)<0$ and finite amplitude $|\Psi_{EX}(z)|^2=|\Phi_{EX}|^2$, as illustrated in Fig. 11. Such an extreme asymmetry between the cases of forward and backward incidence justifies the term *unidirectional freezing* for what happens in a semi-infinite unidirectional slab.

The effect of unidirectional freezing proves to be rather robust when some physical or geometrical parameters of the original unidirectional array are slightly altered. For instance, when the relative thickness $\rho=F/A$ of the layers in the periodic structure in Fig. 2 is increased or decreased by a third [the respective modified dispersion relations are presented in

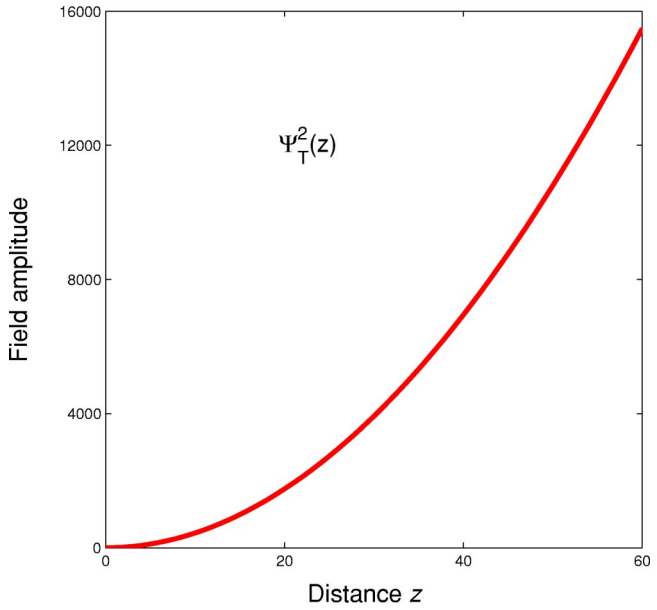

FIG. 10. Amplitude $|\Psi_T(z)|^2$ of electromagnetic field inside unidirectional slab vs the distance z (in units of L) from the slab surface; the frequency ω coincides with the frozen mode frequency ω_0. Polarization of the forward incident wave is linear, with $\vec{E}||x$ [compare with Fig. 8(a)].

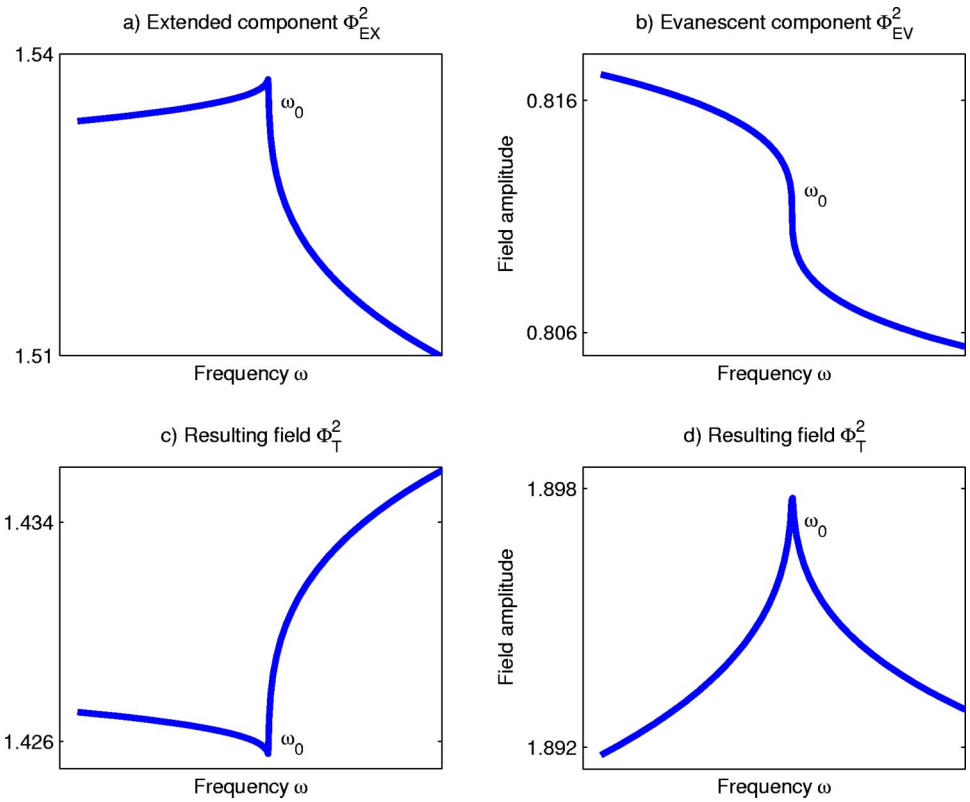

FIG. 11. The amplitude of electromagnetic field Φ_T and its extended (Φ_{EX}) and evanescent (Φ_{EV}) components at the surface of semi-infinite unidirectional slab in Fig. 6 for the case of *backward* incidence: (a) extended contribution $|\Phi_{EX}|^2$ for $\vec{E}\|y$; (b) evanescent contribution $|\Phi_{EV}|^2$ for $\vec{E}\|y$; (c) the resulting field amplitude $|\Phi_T|^2=|\Phi_{EX}+\Phi_{EV}|^2$ for $\vec{E}\|y$; (d) the resulting field amplitude $|\Phi_T|^2$ for $\vec{E}\|x$.

Figs. 3(a) and (b), respectively], the frozen mode blurs, but the surge in electromagnetic field amplitude inside the slab remains quite significant—more than an order of magnitude.

In Sec. IV, we consider the transmittance of a finite gyrotropic photonic slab, which is a finite fragment of a unidirectional photonic crystal. As long as the number of layers constituting a finite slab is small, the electromagnetic properties of the slab does not show any indication of the unidirectionality of the respective infinite or semi-infinite periodic stacks. But when the number N of the elementary fragments L in Fig. 2 is large, the finite slab does show some distinct behavior in the vicinity of the frozen mode frequency ω_0. For instance, the dependence of the slab transmittance on the polarization of the incident radiation is similar to that of the semi-infinite slab. In Figs. 12(a) and (b) one can see that for certain elliptical polarization of the forward incident radiation, the thick unidirectional slab becomes virtually transparent in the vicinity of the frozen mode frequency ω_0. This particular polarization coincides with that shown in Fig. 7(c) and provides the maximal forward transmittance τ_e of the respective semi-infinite slab. In addition to this, both the thick finite slab and the respective unidirectional semi-infinite stack become totally reflective in the vicinity of ω_0, if the polarization of the incident wave is orthogonal to the previous one, as shown in Figs. 7(d) and 12(b), respectively.

II. TRANSVERSE ELECTROMAGNETIC WAVES IN PERIODIC GYROTROPIC MEDIA: ELECTROMAGNETIC UNIDIRECTIONALITY.

This section starts with a brief discussion of bulk electromagnetic properties of gyrotropic periodic layered structures. We consider the basic features of extended and evanescent eigenmodes characteristic of nonreciprocal periodic arrays. Particular attention is given to the effect of unidirectionality. The results of this section are used in the following study of the electromagnetic properties of unidirectional slabs.

A. Definitions and notations

Electromagnetic properties of gyrotropic layered media have been a subject of numerous publications (see, for example Refs. 10–16, and references therein). Our objective here is to introduce those concepts, definitions, and notations, which are necessary for understanding the electromagnetic properties of unidirectional photonic crystals. We consider the simplest and the most important case of layered dielectric media, which supports transverse electromagnetic waves with alternating field components

$$\vec{E}(z),\ \vec{H}(z),\ \vec{D}(z),\ \vec{B}(z)\perp\vec{z}. \tag{15}$$

The direction z of wave propagation is normal to the layers, as shown in Fig. 5. In such a case, the time harmonic Maxwell equations

$$\nabla\times\vec{E}(\vec{r})=\frac{i\omega}{c}\vec{B}(\vec{r}),\ \ \nabla\times\vec{H}(\vec{r})=-\frac{i\omega}{c}\vec{D}(\vec{r}) \tag{16}$$

can be recast as

$$\hat{\sigma}\frac{\partial}{\partial z}\vec{E}(z)=\frac{i\omega}{c}\vec{B}(z),\ \ \hat{\sigma}\frac{\partial}{\partial z}\vec{H}(z)=-\frac{i\omega}{c}\vec{D}(z), \tag{17}$$

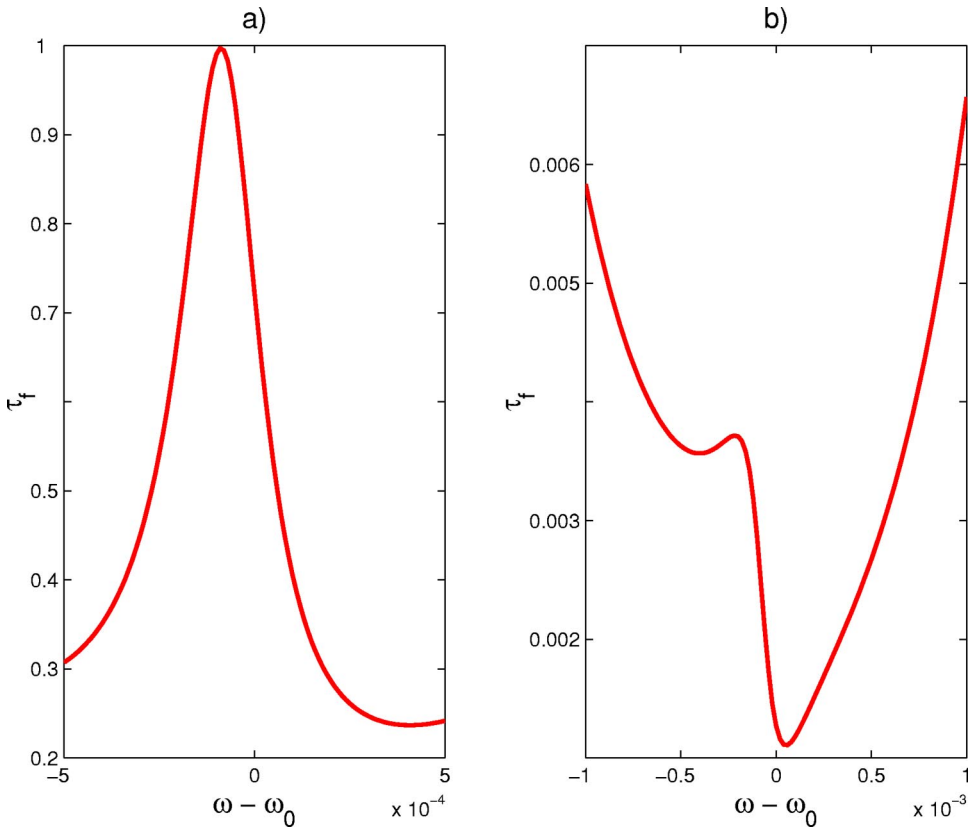

FIG. 12. Forward transmittance of a thick unidirectional slab with $N=32$ in the vicinity of the frozen mode frequency ω_0. The elliptical polarization of the incident wave is: (a) the same as in Fig. 7(c), that provides the maximal transmittance; (b) the same as in Fig. 7(d), that provides total reflectance in both cases. Small deviation of the extreme points from $\omega=\omega_0$ is due to a finite thickness of the slab.

where, in accordance with Eq. (15), all the fields are two-dimensional vectors lying in the x-y plane and

$$\hat{\sigma}=\begin{bmatrix}0 & -1\\ 1 & 0\end{bmatrix}.$$

The transverse alternating electric and magnetic fields $\vec{E}(z)$ and $\vec{H}(z)$ in Eq. (17) are related to the electric and magnetic inductions $\vec{D}(z)$ and $\vec{B}(z)$ by common linear constitutive relations

$$\vec{D}(z)=\hat{\varepsilon}(z)\vec{E}(z),\quad \vec{B}(z)=\hat{\mu}(z)\vec{H}(z). \tag{18}$$

The Hermitian anisotropic tensors

$$\hat{\varepsilon}(z)=\begin{bmatrix}\varepsilon_{xx}(z) & \varepsilon_{xy}(z)\\ \varepsilon^*_{xy}(z) & \varepsilon_{yy}(z)\end{bmatrix},\quad \hat{\mu}(z)=\begin{bmatrix}\mu_{xx}(z) & \mu_{xy}(z)\\ \mu^*_{xy}(z) & \mu_{yy}(z)\end{bmatrix} \tag{19}$$

are frequency dependent and take different values in different layers of the stack. The substitution of Eq. (18) into Eq. (17) gives

$$\hat{\sigma}\frac{\partial}{\partial z}\vec{E}(z)=\frac{i\omega}{c}\hat{\mu}(z)\vec{H}(z);\quad \hat{\sigma}\frac{\partial}{\partial z}\vec{H}(z)=-\frac{i\omega}{c}\hat{\varepsilon}(z)\vec{E}(z). \tag{20}$$

The fields $\vec{E}(z)$ and $\vec{H}(z)$ are continuous functions of z, even if $\hat{\varepsilon}(z)$ and $\hat{\mu}(z)$ along with $\vec{D}(z)$ and $\vec{B}(z)$ are not.

The reduced Maxwell equations (20) can also be recast in a compact form,

$$\hat{M}(z)\Psi(z)=\omega\Psi(z), \tag{21}$$

where

$$\Psi(z)=\begin{bmatrix}E_x(z)\\ E_y(z)\\ H_x(z)\\ H_y(z)\end{bmatrix},\qquad \hat{M}(z)=\frac{c}{i}\begin{bmatrix}0 & \hat{\mu}^{-1}(z)\hat{\sigma}\\ -\hat{\varepsilon}^{-1}(z)\hat{\sigma} & 0\end{bmatrix}\frac{\partial}{\partial z}. \tag{22}$$

The transfer matrix of a layered structure

The transfer-matrix formalism is particularly useful in electrodynamics of layered media composed of anisotropic and/or gyrotropic layers. Below we introduce the basic definitions and notations, consistent with those of Ref. 10. More information on the subject can be found in Refs. 13–16, and references therein.

The reduced time-harmonic Maxwell equations (21) constitute a system of four ordinary linear differential equations of the first order. Its general solution is a linear superposition of four eigenmodes,

$$\Psi(z)=C_1\Psi_1(z)+C_2\Psi_2(z)+C_3\Psi_3(z)+C_4\Psi_4(z). \tag{23}$$

The four coefficients C_i in Eq. (23) can be uniquely related to the four transverse field components (22) at a given point z,

$$\Psi(z)=\hat{W}(z)\begin{bmatrix} C_1 \\ C_2 \\ C_3 \\ C_4 \end{bmatrix}, \tag{24}$$

where $\hat{W}(z)$ is a nonsingular 4×4 matrix

$$\hat{W}(z)=[\Psi_1(z)\ \ \Psi_2(z)\ \ \Psi_3(z)\ \ \Psi_4(z)] \tag{25}$$

composed of the column vectors $\Psi_i(z)$ from Eq. (23). The equality (24) yields a one-to-one correspondence between the electromagnetic field components $\Psi(z)$ at any two different locations z_1 and z_2,

$$\Psi(z_2)=\hat{\mathbf{T}}(z_2,z_1)\Psi(z_1), \tag{26}$$

where the 4×4 matrix

$$\hat{\mathbf{T}}(z_2,z_1)=\hat{W}(z_2)\hat{W}^{-1}(z_1) \tag{27}$$

is referred to as the transfer matrix.[26]

In homogeneous media, the transfer matrix (26) has translation symmetry

$$\hat{T}(z_2-z_1)=\hat{\mathbf{T}}(z_2,z_1), \tag{28}$$

where $\hat{T}(z)=\hat{T}^{-1}(-z)$. In addition, in homogeneous materials without linear magnetoelectric effect, the matrix $\hat{T}(z)$ and $\hat{T}^{-1}(z)$ are similar,

$$\hat{T}(z)=U\hat{T}^{-1}(z)U^{-1}, \tag{29}$$

implying that

$$\det\hat{T}(z)=1. \tag{30}$$

We also introduce the transfer matrix of the mth homogeneous layer $\hat{T}_m=\hat{T}(z_m)$, where z_m is the layer thickness. The single-layer transfer matrix $\hat{T}_m$ depends on the layer thickness z_m and material tensors $\hat{\varepsilon}_m$ and $\hat{\mu}_m$. The explicit expressions for the $\hat{T}$ matrices of anisotropic and gyrotropic layers are rather cumbersome, and those we use are presented in Appendix A.

The T matrix of a stack of layers is the product of the matrices T_m constituting the stack

$$\hat{T}_S=\prod_m \hat{T}_m. \tag{31}$$

Equations (30) and (31) imply that

$$\det\hat{T}_S=1 \tag{32}$$

for an arbitrary stack. At the same time, the similarity relation

$$\hat{T}_S=U\hat{T}_S^{-1}U^{-1}, \tag{33}$$

analogous to Eq. (29), may not hold for some gyrotropic stacks composed of three or more layers. This is directly related to the phenomenon of spectral asymmetry (1). For an extended discussion see the next subsection.

B. Extended and evanescent modes in nonreciprocal periodic stacks

1. Characteristic equation

Bloch solutions for the Maxwell equations (20) in a periodic medium satisfy

$$\Psi_k(z+L)=e^{ikL}\Psi_k(z), \tag{34}$$

where L is the length of the primitive cell of the periodic stack, k is the Bloch wave vector (2), and $\Psi_k(z)$ is the respective column vector (22). The quasimomentum k is defined uniquely up to a multiple of $2\pi/L$.

It follows from the definition (26) of the T matrix that

$$\Psi_k(z+L)=\hat{\mathbf{T}}(z+L,z)\Psi_k(z). \tag{35}$$

Comparing Eqs. (35) and (34) we get at $z=0$

$$\hat{T}_L\Phi_k=e^{ikL}\Phi_k, \tag{36}$$

where $\hat{T}_L=\hat{\mathbf{T}}(L,0)$ is the T matrix of the primitive cell of the periodic stack, while $\Phi_k=\Psi_k(0)$ is one of the four Bloch solutions $\Psi_k(z)$ for the reduced Maxwell equations (20) at $z=0$.

Equation (36) implies that the Bloch eigenvectors Φ_k uniquely relate to those of the transfer matrix $\hat{T}_L$. The respective four eigenvalues

$$\zeta_i=e^{ik_iL},\ \ i=1,2,3,4 \tag{37}$$

of $\hat{T}_L$ are the roots of the characteristic equation

$$\det(\hat{T}_L-\zeta\hat{I})\equiv F(\zeta)=\zeta^4+P_3\zeta^3+P_2\zeta^2+P_1\zeta+1=0, \tag{38}$$

where, according to Ref. 10,

$$P_1=P_3^*,\ \ P_2=P_2^*. \tag{39}$$

Introducing the real coefficients

$$R=\mathrm{Re}\,P_1,\ \ P=\mathrm{Im}\,P_1, \tag{40}$$

we recast Eq. (38) as

$$F(\zeta)=\zeta^4+(R-iP)\zeta^3+P_2\zeta^2+(R+iP)\zeta+1=0 \tag{41}$$

or, in the more symmetrical form,

$$M(\zeta)=\zeta^{-2}F(\zeta)=\zeta^2+(R-iP)\zeta+P_2+(R+iP)\zeta^{-1}+\zeta^{-2}=0. \tag{42}$$

Plugging

$$\zeta=\cos(kL)+i\sin(kL)$$

in Eq. (42) yields yet another form of the characteristic equation

$$M(k) = -2 + P_2 + 2R\cos(kL) + 2P\sin(kL) + 4\cos^2(kL) = 0, \tag{43}$$

where all the coefficients are now real.

2. Extended and evanescent solutions

The coefficients of the characteristic equation are expressed in terms of the elements of the matrix $\hat{T}_L$. Those elements are functions of the physical parameters of the constitutive layers and the frequency ω. For any given frequency ω, the characteristic equation defines a set of four values $\{\zeta_1,\zeta_2,\zeta_3,\zeta_4\}$, or equivalently, $\{k_1,k_2,k_3,k_4\}$. Real k (roots with $|\zeta|=1$) correspond to propagating Bloch waves (extended modes), while complex k (roots with $|\zeta|\neq 1$) correspond to evanescent modes. Evanescent modes are relevant near photonic crystal boundaries and other structural irregularities.

The characteristic equation (42) implies that for any given frequency ω,

$$\text{if } \zeta \text{ is a root, then } 1/\zeta^* \text{ is also a root} \tag{44}$$

or, equivalently,

$$\text{if } k \text{ is a solution, then } k^* \text{ is also a solution.} \tag{45}$$

In view of the statement (44), one has to consider three different situations. The first possibility,

$$|\zeta_1|=|\zeta_2|=|\zeta_3|=|\zeta_4|=1, \tag{46}$$

or, equivalently,

$$k_1\equiv k_1^*,\ k_2\equiv k_2^*,\ k_3\equiv k_3^*,\ k_4\equiv k_4^*,$$

relates to the case of all four Bloch eigenmodes being extended (see, for instance, the frequency range

$$0<\omega<\omega_a \tag{47}$$

in Fig. 1).

The second possibility,

$$|\zeta_1|=|\zeta_2|=1;\ \ \zeta_4=1/\zeta_3^*;\ \text{ where }\ |\zeta_3|,|\zeta_4|\neq 1, \tag{48}$$

or, equivalently

$$k_1=k_1^*,\ k_2=k_2^*,\ k_3=k_4^*,\ \text{ where }\ k_3\neq k_3^*,\ k_4\neq k_4^*,$$

relates to the case of two extended and two evanescent modes (the frequency range

$$\omega_a<\omega<\omega_b \tag{49}$$

in Fig. 1).

The last possibility,

$$\zeta_2=1/\zeta_1^*;\ \ \zeta_4=1/\zeta_3^*;\ \text{ where }\ |\zeta_1|,|\zeta_2|,|\zeta_3|,|\zeta_4|\neq 1, \tag{50}$$

or, equivalently,

$$k_1=k_2^*,\ k_3=k_4^*,\ \text{ where }\ k_1\neq k_1^*,\ k_2\neq k_2^*,\ k_3\neq k_3^*, k_4\neq k_4^*,$$

relates to the case of a frequency gap, when all four Bloch eigenmodes are evanescent (the frequency range

$$\omega_b<\omega \tag{51}$$

in Fig. 1).

Equation (32) implies that in all cases

$$\zeta_1\zeta_2\zeta_3\zeta_4=1 \tag{52}$$

or, equivalently

$$k_1+k_2+k_3+k_4\equiv 0. \tag{53}$$

C. Spectral symmetry vs spectral asymmetry

If all the coefficients in the characteristic equation (38) are real [that amounts to $P=0$ in Eq. (40)], then for a given frequency ω

$$\{\zeta_1,\zeta_2,\zeta_3,\zeta_4\}=\{\zeta_1^*,\zeta_2^*,\zeta_3^*,\zeta_4^*\}, \tag{54}$$

or, in terms of the Bloch wave vectors

$$\text{if }\ P=0,\ \text{ then }\ \{k_1,k_2,k_3,k_4\}=\{-k_1^*,-k_2^*,-k_3^*,-k_4^*\}. \tag{55}$$

Observe that the relation (54) together with Eq. (44) ensure similarity of the matrix $\hat{T}_L$ and $\hat{T}_L^{-1}$,

$$\text{if }\ P=0, \text{ then }\ \hat{T}_L=U\hat{T}_L^{-1}U^{-1}.$$

Conversely

$$\text{if }\ P\neq 0,\ \text{ then }\ \hat{T}_L\neq U\hat{T}_L^{-1}U^{-1}\ \text{ for any } U.$$

In terms of the dispersion relation $\omega(k)$, the relation (55) together with Eq. (45) imply the spectral reciprocity (*spectral symmetry*) of the Bloch eigenmodes,

$$\text{if } P=0 \text{ then}$$

$$\{\omega(k_1),\omega(k_2),\omega(k_3),\omega(k_4)\} = \{\omega(-k_1),\omega(-k_2),\omega(-k_3),\omega(-k_4)\}. \tag{56}$$

In view of the symmetry consideration of Ref. 10, the relation (56) holds for all nonmagnetic and for the majority of magnetic photonic crystals.

The appearance of complex coefficients P_i in Eq. (38) [that amounts to $P\neq 0$ in Eq. (40)] leads to violation of the relation (55) for a given frequency ω,

$$\text{if }\ P\neq 0 \text{ then }\ \{k_1,k_2,k_3,k_4\}\neq\{-k_1^*,-k_2^*,-k_3^*,-k_4^*\}, \tag{57}$$

which in terms of the dispersion relation $\omega(k)$ implies the *spectral asymmetry*

$$\text{if }\ P\neq 0\ \text{ then }\ \{\omega(k_1),\omega(k_2),\omega(k_3),\omega(k_4)\}\neq\{\omega(-k_1),\omega(-k_2),\omega(-k_3),\omega(-k_4)\}. \tag{58}$$

A simplified definition of the spectral asymmetry is given by Eq. (1), where k is presumed real.

Regardless of the spectral symmetry or asymmetry, the evanescent modes (those with $k \neq k^*$), if then exist, must comply with the relation

$$\{\omega(k_1), \ldots\} \equiv \{\omega(k_1^*), \ldots\} \tag{59}$$

following from Eq. (44).

A specific numerical example of asymmetric electromagnetic spectrum is shown in Fig. 1. The physical parameters of the corresponding periodic stack are chosen so that at a certain frequency ω_0 the dispersion relation $\omega(k)$ of one of the spectral branches develops a stationary inflection point. The corresponding frequency is associated with the electromagnetic unidirectionality. In the next subsection, we take a closer look at this particular situation.

D. Stationary inflection point

The dispersion relation $\omega(k)$ of an arbitrary periodic stack is determined by the characteristic equation (41), where the coefficients R, Q, and P are functions of the frequency ω. Using the characteristic equation (41), we can define the stationary inflection point $\zeta_0 = \exp(ik_0 L)$ in Eq. (3) as one satisfying

$$F(\zeta_0) = 0, \;\; F'_\zeta(\zeta_0) = 0, \;\; F''_{\zeta\zeta}(\zeta_0) = 0 \tag{60}$$

with an additional condition

$$F'''_{\zeta\zeta\zeta}(\zeta_0) \neq 0. \tag{61}$$

Equations (60) impose certain relations upon the values R_0, Q_0, and P_0 of the frequency dependent coefficients R, Q, and P at $\omega = \omega_0$. Those relations require ζ_0 to be a triple root of the characteristic polynomial $F(\zeta)$ at $\omega = \omega_0$, i.e.,

$$\begin{aligned} F_0(\zeta) &= \zeta^4 + (R_0 - iP_0)\zeta^3 + Q_0\zeta^2 + (R_0 + iP_0)\zeta + 1 \\ &= (\zeta - \zeta_1)(\zeta - \zeta_0)^3 = 0. \end{aligned} \tag{62}$$

In view of Eqs. (52) and (44), the values ζ_0 and ζ_1 are related by

$$\zeta_1 = \zeta_0^{-3}, \;\; |\zeta_0| = |\zeta_1| = 1 \tag{63}$$

or, equivalently,

$$k_1 \equiv -3k_0, \;\; \mathrm{Im}\, k_0 = \mathrm{Im}\, k_1 = 0. \tag{64}$$

A small deviation of the frequency ω from its special value ω_0 changes the coefficients R_0, Q_0, and P_0 in Eq. (62) and removes the triple degeneracy of the solution ζ_0. Taking into account Eqs. (60) and (61), we have

$$\zeta - \zeta_0 \approx -(6)^{1/3} \left(\frac{\partial F/\partial\omega}{\partial^3 F/\partial\zeta^3} \right)^{1/3}_{\zeta=\zeta_0, \omega=\omega_0} (\omega - \omega_0)^{1/3}\xi,$$

$$\text{where } \xi = 1, e^{2\pi i/3}, e^{-2\pi i/3}, \tag{65}$$

or, in terms of the quasimomentum k,

$$k - k_0 \approx \left(\frac{1}{6}\omega'''(k_0) \right)^{-1/3} (\omega - \omega_0)^{1/3}\xi,$$

$$\text{where } \;\; \xi = 1, e^{i(2\pi/3)}, e^{-i(2\pi/3)}. \tag{66}$$

We can also rearrange Eq. (66) in a different form, which is actually used for further references,

$$\begin{cases} k_{ex} \approx k_0 + 6^{1/3}[\omega'''(k_0)]^{-1/3}(\omega - \omega_0)^{1/3}, \\ k_{ev} \approx k_0 + \dfrac{1}{2}(6)^{1/3}[\omega'''(k_0)]^{-1/3}(\omega - \omega_0)^{1/3} + i\dfrac{\sqrt{3}}{2}6^{1/3}[\omega'''(k_0)]^{-1/3}|\omega - \omega_0|^{1/3}, \\ k_{EV} \approx k_0 + \dfrac{1}{2}(6)^{1/3}[\omega'''(k_0)]^{-1/3}(\omega - \omega_0)^{1/3} - i\dfrac{\sqrt{3}}{2}6^{1/3}[\omega'''(k_0)]^{-1/3}|\omega - \omega_0|^{1/3}. \end{cases} \tag{67}$$

The real quasimomentum k_{ex} in Eq. (67) relates to the extended mode $\Psi_{ex}(z)$, which turns into the frozen mode at $\omega = \omega_0$. The other two solutions, k_{ev} and $k_{EV} = k_{ev}^*$, correspond to a pair of evanescent modes, $\Psi_{ev}(z)$ and $\Psi_{EV}(z)$, with positive and negative imaginary parts, respectively. Those modes are truly evanescent (i.e., have $\mathrm{Im}\, k \neq 0$) only if $\omega \neq \omega_0$. But it does not mean that at $\omega = \omega_0$, the eigenmodes $\Psi_{ev}(z)$ and $\Psi_{EV}(z)$ become extended!

Eigenmodes at frequency ω_0 of stationary inflection point

Consider four eigenvectors,

$$\Phi_{k_1} = \Psi_{k_1}(0), \;\; \Phi_{k_2} = \Psi_{k_2}(0),$$

$$\Phi_{k_3} = \Psi_{k_3}(0), \;\; \Phi_{k_4} = \Psi_{k_4}(0), \tag{68}$$

of the transfer matrix T_L from Eq. (36) in the vicinity of stationary inflection point. As long as $\omega \neq \omega_0$, four eigenvectors (68) comprise two extended and two evanescent Bloch solutions. One of the extended modes (say, Φ_{k_1}) corresponds to the nondegenerate real root $\zeta_1 = e^{ik_1 L}$ of the characteristic equation with the negative group velocity $u(k_1) = \omega'(k_1) < 0$, as shown in Fig. 1. This solution, relating to the backward propagating mode, is of no interest for us. The other three eigenvectors of T_L correspond to three nearly degenerate roots (65). As ω approaches ω_0, those three eigenvectors not only become degenerate, but they also become colinear,

$$\Phi_{k_2} \to \alpha_{2,4}\Phi_{k_4},\ \Phi_{k_3} \to \alpha_{3,4}\Phi_{k_4} \text{ as } \omega \to \omega_0, \tag{69}$$

where $\alpha_{2,4}$ and $\alpha_{3,4}$ are complex scalars. The latter important feature relates to the fact that at $\omega = \omega_0$, the matrix $T_L(\omega_0)$ has a nontrivial Jordan canonical form,

$$T_L(\omega_0) = U \begin{bmatrix} \zeta_1 & 0 & 0 & 0 \\ 0 & \zeta_0 & 1 & 0 \\ 0 & 0 & \zeta_0 & 1 \\ 0 & 0 & 0 & \zeta_0 \end{bmatrix} U^{-1}, \tag{70}$$

and therefore cannot be diagonalized (see, for example, Ref. 17). It is shown rigorously in Appendix B, that the very fact that the T_L eigenvalues display the singularity (65) at $\omega = \omega_0$ implies that the matrix $T_L(\omega_0)$ has the canonical form (70). One of the consequences of Eq. (70) is that the matrix $T_L(\omega_0)$ has only two (not four!) eigenvectors:

(1) Φ_{k_1}, corresponding to the nondegenerate root ζ_1, and

(2) Φ_{k_0}, corresponding to the triple root ζ_0 and describing the frozen mode.

The other two solutions of the Maxwell equation (21) at $\omega = \omega_0$ are general Floquet eigenmodes which do not reduce to the canonical Bloch form. Yet, they can be related to the frozen mode $\Psi_{k_0}(z)$. Indeed, following the standard procedure (see, for example, Ref. 18), consider an extended Bloch solution

$$\Psi_k(z) = \psi_k(z)e^{ikz}, \text{ where } \psi_k(z+L) = \psi_k(L),\ \mathrm{Im}\, k = 0 \tag{71}$$

of the reduced Maxwell equation (21). By definition

$$\hat{M}\Psi_k(z) = \omega(k)\Psi_k(z). \tag{72}$$

Assume that the dispersion relation $\omega(k)$ in Eq. (72) has a stationary inflection point (3) at $k = k_0$. Differentiating Eq. (72) with respect to k gives, in view of Eq. (3),

$$\text{at } k = k_0\text{: } \hat{M}\frac{\partial}{\partial k}\Psi_k(z) = \omega(k)\frac{\partial}{\partial k}\Psi_k(z);\ \hat{M}\frac{\partial^2}{\partial k^2}\Psi_k(z) = \omega(k)\frac{\partial^2}{\partial k^2}\Psi_k(z).$$

This implies that at $k = k_0$, both functions

$$\frac{\partial}{\partial k}\Psi_k(z) = e^{ikz}\frac{\partial}{\partial k}\psi_k(z) + iz\psi_k(z)e^{ikz} \tag{73}$$

and

$$\frac{\partial^2}{\partial k^2}\Psi_k(z) = e^{ikz}\frac{\partial^2}{\partial k^2}\psi_k(z) + ize^{ikz}\frac{\partial}{\partial k}\psi_k(z) - z^2\psi_k(z)e^{ikz} \tag{74}$$

are also eigenmodes of $\hat{M}$ with the same eigenvalue ω_0. Therefore all three solutions (71), (73), and (74) are eigenmodes of $\hat{M}$ with the same eigenvalue ω_0 . For further references we recast those three eigenmodes in the following form:

$$\Psi_{k_0}(z),$$

$$\Psi_{0,1}(z) = \dot{\Psi}_{k_0}(z) + iz\Psi_{k_0}(z), \tag{75}$$

$$\Psi_{0,2}(z) = \ddot{\Psi}_{k_0}(z) + iz\dot{\Psi}_{k_0}(z) - z^2\Psi_{k_0}(z),$$

where

$$\dot{\Psi}_{k_0}(z) = \left(\frac{\partial}{\partial k}\psi_k(z)\right)_{k=k_0} e^{ik_0 z} \text{ and } \ddot{\Psi}_{k_0}(z) = \left(\frac{\partial^2}{\partial k^2}\psi_k(z)\right)_{k=k_0} e^{ik_0 z}$$

are auxiliary Bloch functions (not eigenmodes). Observe that only the first of the three solutions (75) is a canonical Bloch eigenmode [the frozen mode $\Psi_{k_0}(z)$]. The other two solutions diverge as the first and the second power of z, respectively. They are referred to as general Floquet modes.

Deviation of the frequency ω from ω_0 removes the triple degeneracy (70) of the matrix T_L, as can be seen from Eq. (65). The modified matrix T_L can now be reduced to a diagonal form with the set (68) of four eigenvectors comprising two extended and two evanescent Bloch solutions.

III. SEMI-INFINITE UNIDIRECTIONAL STACK

A. Transmittance and reflectance of a semi-infinite stack

Consider plane electromagnetic wave $\Psi_I(z)$ impinging normally on the surface of a unidirectional semi-infinite slab, as shown in Fig. 5. In vacuum (at $z < 0$), the electromagnetic field $\Psi_L(z)$ is a superposition of the incident and reflected waves

$$\text{at } z < 0\text{: } \Psi_L(z) = \Psi_I(z) + \Psi_R(z) \tag{76}$$

where

$$\Psi_I(z) = \Phi_I \exp\left(\frac{i\omega}{c}z\right),\ \Psi_R(z) = \Phi_R \exp\left(-\frac{i\omega}{c}z\right), \tag{77}$$

$$\Phi_I=\Psi_I(0)=\begin{bmatrix} E_{I,x} \\ E_{I,y} \\ -E_{I,y} \\ E_{Ix} \end{bmatrix},\quad \Phi_R=\Psi_R(0)=\begin{bmatrix} E_{R,x} \\ E_{R,y} \\ E_{R,y} \\ -E_{R,x} \end{bmatrix}, \tag{78}$$

$\vec{E}_I$ and $\vec{E}_R$ are complex vectors describing two elliptically polarized waves.

The transmitted wave $\Psi_T(z)$ inside the stack is a superposition of two Bloch eigenmodes,

$$\text{at } z>0:\ \Psi_T(z)=\Psi_1(z)+\Psi_2(z). \tag{79}$$

The eigenmodes $\Psi_1(z)$ and $\Psi_2(z)$ can be both extended, one extended and one evanescent, or both evanescent, depending on which of the three cases (46), (48), or (50) we are dealing with. In particular, if the frequency ω lies within the range $\omega_a<\omega<\omega_b$ in Fig. 1, we have the situation (48), and the transmitted electromagnetic wave $\Psi_T(z)$ is a superposition of the extended Bloch eigenmode $\Psi_{ex}(z)$ with group velocity $u>0$ and the evanescent mode $\Psi_{ev}(z)$ with $\mathrm{Im}\,k>0$,

$$\text{at } z>0:\ \Psi_T(z)=\Psi_{ex}(z)+\Psi_{ev}(z). \tag{80}$$

The only exception to Eq. (80) is when the frequency ω exactly coincides with the frequency ω_0 of the frozen mode. In such a case, $\Psi_T(z)$ is a linear combination of the Floquet eigenmodes (75), one of which is extended [the frozen mode $\Psi_{k_0}(z)$] and the other two cannot be expressed in canonical Bloch form (34). In what follows we assume that ω can be arbitrarily close but not equal to ω_0, unless otherwise is explicitly stated.

Extended and evanescent modes inside a periodic gyrotropic medium are defined by Eq. (36). Knowing the Bloch eigenmodes inside the slab and using the standard electromagnetic boundary conditions

$$\Phi_T=\Phi_I+\Phi_R \tag{81}$$

at the slab surface at $z=0$, one can express the amplitudes Φ_T and Φ_R of transmitted and reflected waves in terms of the amplitude and polarization Φ_I of the incident wave. This gives us the transmittance and reflectance coefficients of semi-infinite slab, as well as the electromagnetic field distribution $\Psi_T(z)$ inside the slab, as functions of the incident wave polarization.

The transmittance τ_e and reflectance r_e of semi-infinite slab are defined as

$$\tau_e=\frac{S(\Phi_T)}{S(\Phi_I)},\quad \rho_e=-\frac{S(\Phi_R)}{S(\Phi_I)};\quad \tau_e+\rho_e=1, \tag{82}$$

where

$$S(\Phi)=\frac{c}{4\pi}\langle E_xH_y-E_yH_x\rangle$$

is the energy density flux averaged over the period of oscillations.

B. Overview of the results

A general idea of what happens when a plane electromagnetic wave of the frequency ω close to the frozen mode frequency ω_0 impinges on the surface of a semi-infinite unidirectional slab, is provided by the numerical examples shown in Figs. 7 and 8.

First, the transmittance τ_e of the semi-infinite unidirectional slab remains finite within the frequency range $\omega_a<\omega<\omega_b$, including the frequency ω_0 of the frozen mode, as seen in in Fig. 7. By contrast, the transmittance τ_e of any semi-infinite slab always vanishes in the vicinity of a band edge (see, for example, the vicinity of $\omega=\omega_b$ in Fig. 7). That the incident wave with the frequency ω_0 can freely enter a semi-infinite unidirectional slab, in spite of the fact that the wave group velocity inside the slab vanishes at $\omega=\omega_0$, has far-reaching implications.

Second, the field amplitude inside unidirectional slab can rise by several orders of magnitude in the vicinity of the frozen mode frequency ω_0, as shown in Figs. 8(a) and 10. This remarkable feature will be discussed in great detail later in this section.

Third, in the vicinity of ω_0, the density of mode has much stronger anomaly compared to that of the vicinity of a band edge frequency. This makes all the effects associated with the frozen mode much more robust.

Finally, the transmittance as well as the reflectance coefficients develop a cusplike singularity at $\omega=\omega_0$; the magnitude and the sign of this singularity being dependent on the polarization of the incident wave. In particular, if the incident wave polarization is chosen so that only a single extended mode $\Psi_{ex}(z)$ continues inside the slab [no evanescent contribution to $\Psi_T(z)$], then the transmittance τ_e at $\omega=\omega_0$ drops down to zero, as shown in Fig. 7(d). But, if the incident wave polarization is orthogonal to the previous one [see Fig. 7(c)], the transmittance of the unidirectional slab is maximal. The explanation for such an unusual behavior is given further in this section. Of course, if the incident wave polarization is chosen so that only a single evanescent mode $\Psi_{ev}(z)$ continues inside the slab [no extended contribution to $\Psi_T(z)$], the transmittance of any semi-infinite slab is strictly zero regardless of the frequency ω.

C. Frequency dependence of electromagnetic field amplitude inside unidirectional slab

According to Eq. (80), the transmitted wave $\Psi_T(z)$ inside the stack is a superposition of one extended (nearly frozen) mode $\Psi_{ex}(z)$ and one evanescent mode $\Psi_{ev}(z)$. Since evanescent modes do not transfer energy, the extended mode $\Psi_{ex}(z)$ is solely responsible for the energy flux inside the stack. The energy density W_{ex} associated with the extended $\Psi_{ex}(z)$ can be expressed in terms of its group velocity $u(k)=\omega'(k)$ and the energy density flux $S(\Phi_{ex})$,

$$W_{ex}=S(\Phi_{ex})/\omega'(k),\ \text{ where }\ S(\Phi_{ex})=S(\Phi_T)=\tau_eS(\Phi_I). \tag{83}$$

In line with Eq. (3), in the vicinity of the frozen mode frequency

$$\omega(k)-\omega_0\approx\frac{1}{6}\omega'''(k_0)(k-k_0)^3$$

that gives

$$\omega'(k)\approx\frac{1}{2}\omega'''(k_0)(k-k_0)^2\approx\frac{6^{2/3}}{2}[\omega'''(k_0)]^{1/3}(\omega-\omega_0)^{2/3}. \tag{84}$$

Plugging Eq. (84) into Eq. (83) yields

$$W_{ex}\approx\frac{2}{6^{2/3}}(\tau_e S_I)[\omega'''(k_0)]^{-1/3}(\omega-\omega_0)^{-2/3}, \tag{85}$$

where $S_I=S(\Phi_I)$ is a fixed intensity of the incident wave, τ_e is the transmittance coefficient (82) depending on the incident wave polarization. Formula (85) implies that the amplitude Φ_{ex} of the extended nearly frozen mode inside the stack diverges in the vicinity of the stationary inflection point

$$\Phi_{ex}\sim\sqrt{W_{ex}}\sim\sqrt{\tau_e S_I}[\omega'''(k_0)]^{-1/6}|\omega-\omega_0|^{-1/3}\ \text{ as }\ \omega\to\omega_0. \tag{86}$$

The divergence of the extended mode amplitude Φ_{ex} in the vicinity of the frozen mode frequency ω_0 imposes a similar kind of behavior on the evanescent mode amplitude Φ_{ev}. Indeed, the boundary condition (81) requires that the resulting field amplitude $\Phi_T=\Phi_{ex}+\Phi_{ev}$ at the slab boundary at $z=0$ remains limited to match the sum $\Phi_L=\Phi_I+\Phi_R$ of the incident and reflected waves outside the stack at $z=0$. The relation (81) together with Eq. (86) imply that there is a destructive interference of the extended Φ_{ex} and evanescent Φ_{ev} modes at the stack boundary

$$\Phi_{ex}\approx-\Phi_{ev}\sim(\omega-\omega_0)^{-1/3}\ \text{ as }\ \omega\to\omega_0 \tag{87}$$

so that $\Phi_T=\Phi_{ex}+\Phi_{ev}$ remains limited. The expression (87) is in compliance with the earlier made statement (69) that the column vectors $\Phi_{ex}$and Φ_{ev} become colinear as $\omega\to\omega_0$.

The numerical illustration of the behavior of the field amplitudes $|\Phi_{ex}|^2$, $|\Phi_{ev}|^2$ and $|\Phi_T|^2=|\Phi_{ex}+\Phi_{ev}|^2$ at the slab surface is illustrated in Figs. 9(a)–(c), respectively.

D. Space distribution of electromagnetic field inside unidirectional slab

Since $\Psi_{ex}(z)$ is an extended Bloch eigenmode, its amplitude $|\Psi_{ex}(z)|$ remains constant at $z>0$, while the amplitude of the evanescent contribution $\Psi_{ev}(z)$ to the resulting field $\Psi_T(z)$ decays as

$$\text{at}\quad z>0:\quad |\Psi_{ev}(z)|=|\Phi_{ev}|e^{-z\,\mathrm{Im}\,k_{ev}}. \tag{88}$$

Therefore, as the distance z from the unidirectional slab boundary increases, the destructive interference of the extended and evanescent modes becomes ineffective, and at $z\gg(\mathrm{Im}\,k_{ev})^{-1}$ the only remaining contribution to $\Psi_T(z)$ is the extended nearly frozen mode $\Psi_{ex}(z)$ with huge and independent of z amplitude (86).

Let us consider the above behavior in more detail. According to Eq. (67), in the vicinity of $\omega=\omega_0$,

$$\mathrm{Im}\,k_{ev}\approx\frac{\sqrt{3}}{2}6^{1/3}[\omega'''(k_0)]^{-1/3}|\omega-\omega_0|^{1/3}. \tag{89}$$

Plugging Eq. (89) in Eq. (88) gives

$$\text{at}\ \ z>0:\quad |\Psi_{ev}(z)|\approx|\Phi_{ev}|\left[1-z\frac{\sqrt{3}}{2}6^{1/3}[\omega'''(k_0)]^{-1/3}\times|\omega-\omega_0|^{1/3}+O\left(\frac{z^2|\omega-\omega_0|^{2/3}}{(\omega'''(k_0))^{2/3}}\right)\right],$$

which together with Eqs. (86) and (87) yields the following asymptotic expression for the evanescent mode amplitude as function of ω and z:

$$|\Psi_{ev}(z)|\approx\frac{\sqrt{\tau_e S_I}}{[\omega'''(k_0)]^{1/6}}\left[|\omega-\omega_0|^{-1/3}-z\frac{\sqrt{3}}{2}6^{1/3}[\omega'''(k_0)]^{-1/3}+O\left(\frac{z^2|\omega-\omega_0|^{1/3}}{(\omega'''(k_0))^{2/3}}\right)\right]. \tag{90}$$

Finally, plugging $\Psi_{ex}(z)$ from Eq. (86) and $\Psi_{ev}(z)$ from Eq. (90) into $\Psi_T(z)=\Psi_{ex}(z)+\Psi_{ev}(z)$ yields

$$|\Psi_T(z)|\approx|\Phi_T|+z\frac{\sqrt{\tau_e S_I}}{[\omega'''(k_0)]^{1/2}}\frac{\sqrt{3}}{2}6^{1/3}\quad\text{as}\quad\omega\to\omega_0, \tag{91}$$

where, according to Eq. (87),

$$|\Phi_T|\ll|\Phi_{ex}|\approx|\Phi_{ev}|.$$

The asymptotic expression (91) for $|\Psi_T(z)|$ is consistent with the eigenmode $\Psi_{1,0}(z)$ from Eq. (75), which represents one of the two Floquet-type solutions for the Maxwell equation (21) at $\omega=\omega_0$.

A numerical example of electromagnetic field distribution $|\Psi_T(z)|^2$ inside the semi-infinite unidirectional slab for the frequency ω close to ω_0 is shown in Fig. 8, while the limiting case (91) of $\omega=\omega_0$ is shown in Fig. 10. The relation (91) implies that the resulting field amplitude $|\Psi_T(z)|^2$ increases as the second power of the distance z from the slab surface. It reaches its maximum value of $|\Psi_{ex}(z)|^2\sim(\omega-\omega_0)^{-2/3}$ at $z\gg l$, where

$$l=(\mathrm{Im}\,k_{ev})^{-1}=\frac{2}{\sqrt{3}}6^{-1/3}[\omega'''(k_0)]^{1/3}|\omega-\omega_0|^{-1/3}. \tag{92}$$

There are two exceptions, however, merging into a single one at $\omega=\omega_0$. The first exception occurs when the elliptic polarization of the incident wave is chosen so that it produces just a single extended eigenmode $\Psi_{ex}(z)$ inside the slab [no evanescent contribution to $\Psi_T(z)$]. In this case, $\Psi_T(z)$ reduces to $\Psi_{ex}(z)$, and its amplitude $|\Psi_T(z)|$ remains limited and independent of z. As ω approaches ω_0, the respective transmittance τ_e vanishes in this case, as shown in Fig. 7(d). The second exception occurs when the elliptic polarization of the incident wave is chosen so that it produces

just a single evanescent eigenmode $\Psi_{ev}(z)$ inside the slab [no extended contribution to $\Psi_T(z)$]. In such a case, $\Psi_T(z)$ reduces to $\Psi_{ev}(z)$, and its amplitude $|\Psi_T(z)|$ decays exponentially with z in accordance with Eq. (88). The respective transmittance coefficient τ_e in this latter case is zero regardless of the frequency ω, because evanescent modes do not transfer energy. Importantly, as ω approaches ω_0, the polarizations of the incident wave that produce either a sole extended or a sole evanescent mode become indistinguishable, which is a consequence of the property (69) of the T_L eigenvectors. If Φ_{I0} is such a polarization of the incident wave, the maximal transmittance is reached when the incident wave polarization is orthogonal to Φ_{I0} [see Fig. 7(c)].

Let us see what happens if the degree of spectral asymmetry of the unidirectional periodic stack is very small. In this situation the stationary inflection point k_0, ω_0 in Fig. 1 is very close to the band edge k_b, ω_b. In such a case, the third derivative $\omega'''(k_0)$ along with the transmittance τ_e of the respective unidirectional slab at $\omega=\omega_0$ are also very small. At the same time, the ratio $\tau_e/\omega'''(k_0)$, which according to Eq. (91) determines the electromagnetic field distribution inside the slab at $\omega\to\omega_0$, remains finite even if the quantities τ_e and $\omega'''(k_0)$ vanish. This implies that at $\omega=\omega_0$, the character of the field distribution shown in Fig. 10 does not change qualitatively even if

$$\omega'(k_0)=\omega''(k_0)=\omega'''(k_0)=0, \quad \omega''''(k_0)\neq 0.$$

Such a situation, however, corresponds to a degenerate band edge, rather than to a stationary inflection point (3).

E. Backward wave incidence on a semi-infinite unidirectional slab

Consider now electromagnetic wave incident on the surface of the same unidirectional slab from the opposite direction, as shown in Fig. 6. Such a situation is similar to that of the forward incidence on the *reversed* slab, which can be obtained from the original unidirectional slab in Fig. 2 by changing the sign of the F layers magnetization or by changing the sign of the misalignment angle $\varphi=\varphi_1-\varphi_2$ of the anisotropic dielectric layers.

Except for some obvious modifications involving the substitution $z\to -z$, formulas (76)–(83) still apply here. In particular, if the frequency ω lies within the range $\omega_a<\omega<\omega_b$ in Fig. 1, the transmitted electromagnetic wave $\Psi_T(z)$ inside the slab is a superposition of the extended Bloch eigenmode $\Psi_{EX}(z)$ with the group velocity $u<0$ and the evanescent mode $\Psi_{EV}(z)$ with $\mathrm{Im}\,k<0$,

$$\text{at } z<0: \quad \Psi_T(z)=\Psi_{EX}(z)+\Psi_{EV}(z). \tag{93}$$

This expression is similar to Eq. (80), except that it involves the other pair of the four Bloch eigenmodes. In the case of backward incidence, the nearly frozen mode $\Psi_{ex}(z)$ does not contribute to $\Psi_T(z)$ inside semi-infinite slab. Instead, the extended contribution to the resulting transmitted electromagnetic field $\Psi_T(z)$ is now $\Psi_{EX}(z)$, which remains a regular extended mode with finite negative group velocity even at $\omega=\omega_0$. It does not mean, however, that the slab unidirectionality does not manifest itself in the case of the backward incidence. Indeed, the evanescent contribution $\Psi_{EV}(z)$ to $\Psi_T(z)$ still displays a singularity at $\omega=\omega_0$, although its amplitude now remains limited even at $\omega=\omega_0$.

Let us take a closer look at this situation. The complex wave vector k_{EV} related to $\Psi_{EV}(z)$ has negative imaginary part and is defined in Eq. (67),

$$k_{EV}\approx k_0+\frac{6^{1/3}}{2}[\omega'''(k_0)]^{-1/3}[(\omega-\omega_0)^{1/3}-i\sqrt{3}|\omega-\omega_0|^{1/3}].$$

Its singularity at $\omega=\omega_0$ leads to a cusplike anomaly in frequency dependence of the backward transmittance of semi-infinite unidirectional slab, similar to what we already saw in the case of forward incidence (see Fig. 7). But there is a crucial difference: the propagating mode amplitude $|\Psi_{EX}(z)|=|\Phi_{EX}|$ now remains limited in the whole frequency range $\omega_a<\omega<\omega_b$, including the frozen mode frequency ω_0, as shown in Fig. 11. By contrast, in the case of forward incidence, the propagating mode amplitude $|\Psi_{ex}(z)|=|\Phi_{ex}|$ along with the field amplitude $|\Psi_T(z)|$ inside the stack rises enormously in the vicinity of the frozen mode frequency ω_0, as shown in Fig. 9(a). This striking difference between the cases of forward and backward incidence can be attributed to the frozen mode.

IV. A FINITE UNIDIRECTIONAL SLAB

Strictly speaking, the concept of unidirectionality applies to infinite or semi-infinite periodic stacks. But in reality, if we have a finite slab, which is a sufficiently large fragment of a periodic unidirectional stack, the results of the previous section can still be relevant. Let N be the number of the primitive cells in the slab, so that the slab thickness D is equal to LN. The approximation of infinite or semi-infinite stack applies if

$$1\ll(L\Delta k)^{-1}\ll N, \tag{94}$$

where Δk is the spectral width of the wave packet. In such a case, the interference of the pulses produced by internal reflections from the two opposite slab boundaries can be ignored. The results of the previous section relate to this particular case.

In this section we consider a different situation when

$$1\ll N\ll(L\Delta k)^{-1}. \tag{95}$$

In particular, we can refer to the limiting case $\Delta k=0$ of a strictly monochromatic incident wave. In this latter case the approximation of infinite or semi-infinite slab does not hold for any finite N, due to multiple internal reflections form the two slab boundaries. The electromagnetic field $\Psi_T(z)$ inside the slab is now a superposition of all four Bloch eigenmodes $\Psi_{k_i}(z)$, $i=1,2,3,4$ for any given frequency ω regardless of the direction of the incident wave propagation outside the slab. By contrast, in the case (94) of semi-infinite slab, there are only two Bloch contributions (79) to $\Psi_T(z)$. At the same time, we expect some noticeable electromagnetic abnormalities even in the limiting case (95), provided that the number N of the elementary fragments L in the slab is large enough.

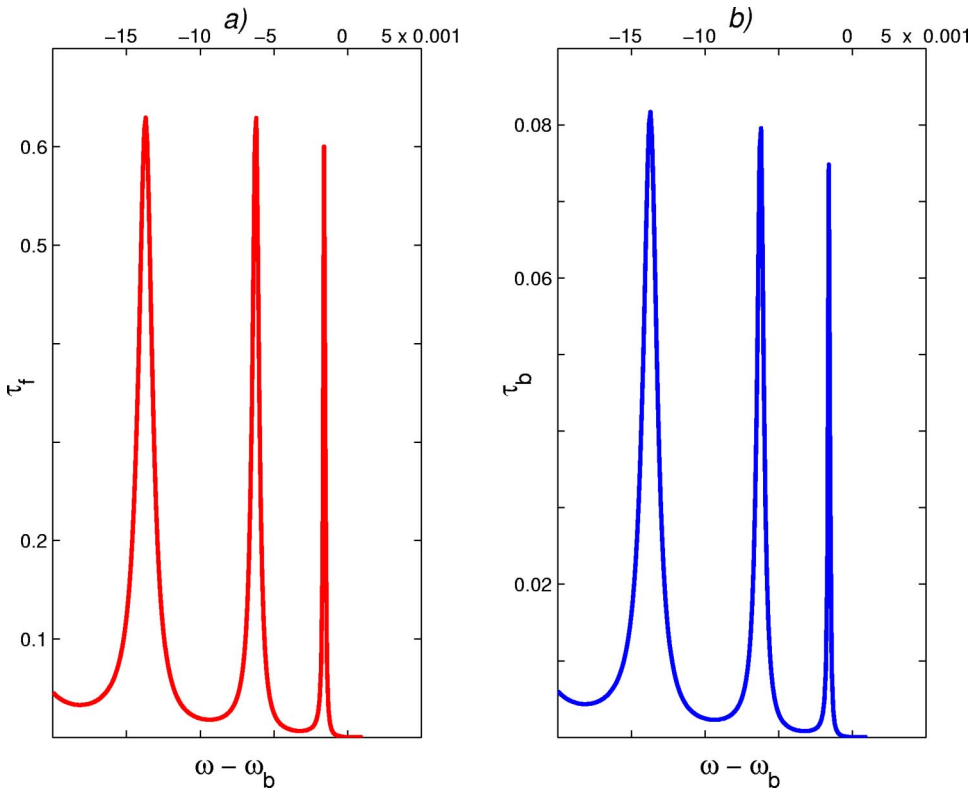

FIG. 13. Forward (a) and backward (b) tramittance of the finite unidirectional slab with $N=32$. The frequency ω lies in the vicinity of the lowest band edge ω_b in Fig. 1.

Transmittance of a finite unidirectional slab

The transmittance of an arbitrary finite slab can be expressed directly in terms of the transfer matrix T_N of the slab, which in our case is defined by

$$T_N=(T_L)^N. \tag{96}$$

Indeed, the relation

$$\Psi(D)=T_N\Psi(0) \tag{97}$$

together with the pair of boundary conditions

$$\Psi(0)=\Psi_I(0)+\Psi_R(0), \quad \Psi(D)=\Psi_P(D) \tag{98}$$

allow us to express both the reflected wave $\Psi_R(0)$ and the wave $\Psi_P(D)$ passed through the slab, in terms of a given incident wave $\Psi_I(0)$ from Eq. (78) and the elements of the transfer matrix T_N. It also gives the transmittance/reflectance coefficients of the slab defined as

$$\tau_N=\frac{|\Psi_P(D)|^2}{|\Psi_I(0)|^2}, \quad \rho_N=\frac{|\Psi_R(0)|^2}{|\Psi_I(0)|^2}; \quad \tau_N+\rho_N=1, \tag{99}$$

respectively. The above procedure is commonly used for computation of the transmittance/reflectance coefficients of magnetic layered structures (see, for example, Refs. 13–16 and references therein). Notice that as long as we are dealing with strictly monochromatic incident wave ($\Delta k=0$), the transmittance/reflectance coefficients (82) of a semi-infinite slab cannot be viewed as the limiting case $N\to\infty$ of the transmittance/reflectance coefficients (99) of a finite slab.

Since the transmittance computation for a finite slab with a given transfer matrix T_N is a well-established procedure, we skip the details and turn to the physical results. If a slab is composed of just a few elementary cells L in Fig. 2, its transmittance does not show any peculiarities in the vicinity of the frozen mode frequency ω_0. As the number N increases, the electromagnetic abnormalities in the vicinity of the frozen mode frequency become more and more distinct. In Figs. 12 and 13 we present some numerical results for the transmittance of a finite unidirectional slab comprising $N=32$ identical elementary fragments L. This number of layers appears to be large enough to display all the qualitative features characteristic of a very thick unidirectional slab. The most distinguishable new feature is that the forward (left-to-right) and the backward (right-to-left) transmittance coefficients do show a strong abnormality in the vicinity of the frozen mode frequency ω_0. In particular, if the elliptic polarization of the incident wave coincides with that of the maximal transmittance of the respective semi-infinite slab [see Fig. 7(c)], the finite slab becomes totally transparent, as shown in Fig. 12(a). A small difference between the frequency of total transmittance and ω_0 is due to a finite thickness of the slab.

At frequencies not too close to ω_0, the electromagnetic properties of a unidirectional slab are not much different from those of regular magnetic stacks (see, for example,[13–16] and references therein). In particular, at certain polarizations of the incident wave, a finite slab displays both, forward and backward resonant transmittance even in the close proximity of the band edges, as shown in Fig. 13.

V. SUMMARY

As we have shown, the phenomenon of unidirectionality in magnetic photonic crystals is always associated with the

existence of special propagating mode with zero group velocity $\omega_k'(k)$ and its derivative $\omega_{kk}''(k)$. We call it the frozen mode. At first glance, the fact that the frozen mode has zero group velocity will bring some similarity between the vicinity of the frozen mode frequency (at $\omega \approx \omega_0$), and the vicinity of the photonic band edge (say, at $\omega \approx \omega_b$). Indeed, in either situation the propagating electromagnetic wave inside the periodic medium slows down dramatically, although in the frozen mode case the slowdown occurs only in one of the two opposite directions (the unidirectionality). But in fact, the dissimilarity between the two situations does not reduce just to the phenomenon of unidirectionality.

The most graphic manifestation of the fundamental difference between the vicinity of the frozen mode frequency ω_0 and the vicinity of a band-gap frequency ω_b is provided by the simple and important case of electromagnetic wave incidence on the surface of a semi-infinite slab shown in Fig. 5. In a broad vicinity of the frozen mode frequency, including the point $\omega = \omega_0$, the incident radiation enters the semi-infinite slab with little reflectance. By contrast, at $\omega \approx \omega_b$ the same semi-infinite slab reflects 100% of the incident radiation. This crucial difference is illustrated in Figs. 7(a)–(c). In fact, the only way to transmit the radiation at frequency $\omega \approx \omega_b$ inside the slab is to make the slab thin enough to ensure strong interference after multiple reflections from the two slab boundaries (see, for example, Ref. 21 and references therein).

What happens in a photonic crystal at frequencies close to the frozen mode frequency ω_0 is that the pulse freely enters the slab, where it slows down by, say, two or three orders of magnitude and increases in amplitude proportionally. Then the pulse slowly continues through the slab without losing its distinct individuality until it reaches the opposite boundary or gets converted or absorbed inside the slab. The fact that in the vicinity of the stationary inflection point (3) (i.e., at $\omega \approx \omega_0$) the space dispersion $\omega_{kk}''(k)$ vanishes, further contributing to the pulse stability. *Nothing like that can occur in any regular photonic crystal, not supporting the frozen mode*. In addition, the electromagnetic density of mode displays a much stronger anomaly at $\omega \approx \omega_0$ compared to any other location in the Brillouin zone including the band edges. The latter circumstance must facilitate the observation and utilization of the frozen mode phenomena. The above unique features, in a combination with the relative simplicity of the multilayered structures, can make unidirectional photonic crystals very attractive for practical purposes. This may include:

- various nonlinear applications (see, for example, Refs. 22 and 21, and references therein), which can take advantage of huge amplitude of the frozen mode, in a combination with high transmittance and high density of modes at the respective frequency;
- tunable delay lines, utilizing low group velocity of the frozen mode, as well as its low dispersion ($\omega_{kk}'' \approx 0$) and high transmittance of the slab;
- electromagnetic nonreciprocal devices, utilizing the phenomenon of unidirectionality itself.

ACKNOWLEDGMENT AND DISCLAIMER

The efforts of A. Figotin and I. Vitebskiy were sponsored by the Air Force Office of Scientific Research, Air Force Materials Command, USAF, under Grant No. F49620-01-1-0567. The U.S. Government is authorized to reproduce and distribute reprints for governmental purposes notwithstanding any copyright notation thereon. The views and conclusions contained herein are those of the authors and should not be interpreted as necessarily representing the official policies or endorsements, either expressed or implied, of the Air Force Office of Scientific Research or the U.S. Government.

APPENDIX A: GYROTROPIC STACK WITH THREE-LAYERED CELL

Having studied numerically a number of periodic magnetic stacks with bulk spectral asymmetry, we come to the following conclusion. As long as we restrict ourselves to the lowest spectral band, the electromagnetic dispersion relations with stationary inflection point computed for different stacks appear to be qualitatively similar to each other and to what is shown in Fig. 1. In addition to this, since our prime interest here is with the vicinity of the frozen mode frequency ω_0, all essential electromagnetic features prove to be quite universal and dependent on a single dimensionless parameter ϕ from Eq. (4). In the case of strong spectral asymmetry, ϕ is of the order of magnitude of unity. This circumstance allows us to use any particular numerical example to obtain a complete picture of what is going on in unidirectional photonic crystals in the vicinity of the frozen mode frequency. Example considered in this section represents the simplest and, perhaps, the most practical design of a periodic layered structure with the property of bulk spectral asymmetry (1). This array, shown in Fig. 2, is similar to that considered in Ref. 10. As already noted, a particular choice of the physical parameters of the stack does not matter, as long as it provides a certain value of ϕ.

The **A** layers are described by the following reduced property tensors:

$$\hat{\varepsilon}_{\mathbf{A}} = \begin{bmatrix} \varepsilon_{xx} & \varepsilon_{xy} \\ \varepsilon_{xy} & \varepsilon_{yy} \end{bmatrix} = \begin{bmatrix} \varepsilon + \delta\cos 2\varphi & \delta \sin 2\varphi \\ \delta \sin 2\varphi & \varepsilon - \delta\cos 2\varphi \end{bmatrix},$$

$$\hat{\mu}_{\mathbf{A}} = \begin{bmatrix} \mu_{xx} & \mu_{xy} \\ \mu_{xy} & \mu_{yy} \end{bmatrix} = \begin{bmatrix} \mu + \Delta\cos 2\varphi & \Delta \sin 2\varphi \\ \Delta \sin 2\varphi & \mu - \Delta\cos 2\varphi \end{bmatrix}. \tag{A1}$$

All components of $\hat{\varepsilon}_{\mathbf{A}}$ and $\hat{\mu}_{\mathbf{A}}$ are presumed real. Parameters δ and Δ describe the anisotropy in the xy plane, while the angle φ defines the orientation of the common principle axes of $\hat{\varepsilon}_{\mathbf{A}}$ and $\hat{\mu}_{\mathbf{A}}$ in the xy plane. The misalignment angle $\varphi_1 - \varphi_2$ between the neighboring layers in Fig. 2 must be different from 0 and $\pi/2$. All **A** layers are made of the same dielectric material and have the same thickness A .

The four solutions for the Maxwell equation (21) with material relations (A1) are

$$e^{iq_1z}\Phi_{A1}, e^{-iq_1z}\Phi_{A1}, e^{iq_2z}\Phi_{A2}, e^{-iq_2z}\Phi_{A2}, \tag{A2}$$

where

$$\Phi_{A1}=\begin{bmatrix}\cos\varphi\\ \sin\varphi\\ -\eta_1\sin\varphi\\ \eta_1\cos\varphi\end{bmatrix}, \quad \Phi_{A2}=\begin{bmatrix}-\sin\varphi\\ \cos\varphi\\ -\eta_2\cos\varphi\\ -\eta_2\sin\varphi\end{bmatrix}, \tag{A3}$$

$$q_1=\frac{\omega}{c}n_1=\frac{\omega}{c}\sqrt{(\varepsilon+\delta)(\mu-\Delta)},$$

$$q_2=\frac{\omega}{c}n_2=\frac{\omega}{c}\sqrt{(\varepsilon-\delta)(\mu+\Delta)}, \tag{A4}$$

$$\eta_1=\sqrt{(\varepsilon+\delta)(\mu-\Delta)^{-1}}, \quad \eta_2=\sqrt{(\varepsilon-\delta)(\mu+\Delta)^{-1}}. \tag{A5}$$

Substituting the eigenmodes (A2) into $\hat{W}(z)$ from Eq. (25) and using the definition (27) of the T matrix, we have the following expression for the transfer matrix $\hat{T}_A$ of an individual **A** layer as a function of the layer thickness A and the misalignment angle φ:

$$\hat{T}_A(\varphi,A)=\hat{W}(\varphi,A)\hat{W}^{-1}(\varphi,0), \tag{A6}$$

where

$$\hat{W}(\varphi,A)=\begin{bmatrix}(\cos\varphi)e^{in_1a} & (\cos\varphi)e^{-in_1a} & -(\sin\varphi)e^{in_2a} & -(\sin\varphi)e^{-in_2a}\\ (\sin\varphi)e^{in_1a} & (\sin\varphi)e^{-in_1a} & (\cos\varphi)e^{in_2a} & (\cos\varphi)e^{-in_2a}\\ -\eta_1(\sin\varphi)e^{in_1a} & \eta_1(\sin\varphi)e^{-in_1a} & -\eta_2(\cos\varphi)e^{in_2a} & \eta_2(\cos\varphi)e^{-in_2a}\\ \eta_1(\cos\varphi)e^{in_1a} & -\eta_1(\cos\varphi)e^{-in_1a} & -\eta_2(\sin\varphi)e^{in_2a} & \eta_2(\sin\varphi)e^{-in_2a}\end{bmatrix}, \tag{A7}$$

$$a=\frac{\omega}{c}A. \tag{A8}$$

The **F** layers are ferromagnetic (or ferrimagnetic) with magnetization $\vec{M}_0$ parallel to the z direction; there is no in-plane anisotropy in this case,

$$\hat{\varepsilon}_{\mathbf{F}}=\begin{bmatrix}\epsilon & i\alpha\\ -i\alpha & \epsilon\end{bmatrix}; \quad \hat{\mu}_{\mathbf{F}}=\begin{bmatrix}\mu & i\beta\\ -i\beta & \mu\end{bmatrix}. \tag{A9}$$

The real parameters α and β in Eq. (A9) are responsible for Faraday rotation. All **F** layers have the same thickness F.

The four solutions for the Maxwell equation (21) with material relations (A9) are

$$e^{iq_1z}\Phi_{F1}, e^{-iq_1z}\Phi_{F1}, e^{iq_2z}\Phi_{F2}, e^{-iq_2z}\Phi_{F2}, \tag{A10}$$

where

$$\Phi_{F1}=\begin{bmatrix}1\\ -i\\ i\eta_1\\ \eta_1\end{bmatrix}, \quad \Phi_{F2}=\begin{bmatrix}-i\\ 1\\ -\eta_2\\ -i\eta_2\end{bmatrix}, \tag{A11}$$

$$q_1=\frac{\omega}{c}n_1=\frac{\omega}{c}\sqrt{(\epsilon+\alpha)(\mu+\beta)}, \quad q_2=\frac{\omega}{c}n_2$$

$$=\frac{\omega}{c}\sqrt{(\epsilon-\alpha)(\mu-\beta)}, \tag{A12}$$

$$\eta_1=\sqrt{(\epsilon+\alpha)(\mu+\beta)^{-1}}, \quad \eta_2=\sqrt{(\epsilon-\alpha)(\mu-\beta)^{-1}}. \tag{A13}$$

Substituting the eigenmodes (A10) into $\hat{W}(z)$ from Eq. (25) and using the definition (27) of the T matrix, we have the following expression for the transfer matrix $\hat{T}_F$ of an individual **F** layer as a function of the layer thickness F:

$$\hat{T}_F=\hat{W}(F)\hat{W}^{-1}(0), \tag{A14}$$

where

$$\hat{W}(F)=\begin{bmatrix}e^{in_1f} & e^{-in_1f} & -ie^{in_2f} & -ie^{-in_2f}\\ -ie^{in_1f} & -ie^{-in_1f} & e^{in_2f} & e^{-in_2f}\\ i\eta_1e^{in_1f} & -i\eta_1e^{-in_1f} & -\eta_2e^{in_2f} & \eta_2e^{-in_2f}\\ \eta_1e^{in_1f} & -\eta_1e^{-in_1f} & -i\eta_2e^{in_2f} & i\eta_2e^{-in_2f}\end{bmatrix}, \tag{A15}$$

$$f=\frac{\omega}{c}F. \tag{A16}$$

The T atrices of **F** layers with two opposite signs of $\vec{M}_0$, are related by transposition of the indices 1 and 2.

Having the T matrices of both constitutive layers, one can obtain the explicit expression for the transfer matrix T_L of the three-layered primitive cell in Fig. 2,

$$T_L(\varphi,A,F)=T_A(\varphi_1,A)T_A(\varphi_2,A)T_F(F). \tag{A17}$$

Symbolic analysis of the transfer matrix $T_L(\varphi,A,F)$, as well as the corresponding characteristic equation (38), has been carried out using the computer algebra package of "maple 7."

We have also conducted a number of numerical experiments with this particular gyrotropic stack. When it comes to the vicinity of the frozen mode frequency, the general picture is universal, provided that the dimensionless parameter ϕ from Eq. (4) is not too small. For this reason, all numerical illustrations in this paper refer to a single numerical set of material parameters of the stack chosen as follows:

$$\begin{aligned} &\text{for the } \mathbf{A} \text{ layer:} \quad n_1=5.1,\ \eta_1=5.1,\ n_2=1.1,\ \eta_2=1.1,\\ &\text{for the } \mathbf{F} \text{ layer:} \quad n_1=22.023,\ \eta_1=0.227\,04,\\ &\qquad\qquad\qquad\quad n_2=10.724,\ \eta_2=0.466\,25, \end{aligned} \tag{A18}$$

with the misalignment angle

$$\varphi_1-\varphi_2=\pi/4.$$

The numerical values (A18) are practically available at frequencies below 10^{12}Hz, but otherwise they are chosen randomly. On the other hand, having set the material parameters (A18), we must find the exact values of the layer thicknesses so that at some frequency ω_0 the stack develops a stationary inflection point (3) and therefore displays the property of unidirectionality. For the numerical values (A18) we found

$$\begin{aligned} \rho_0&=F/A=0.009\,536\,025\,9,\\ \Omega_0&=L\omega_0/c=0.607\,676\,756,\\ K_0&=k_0L=2.632\,925\,94 \end{aligned} \tag{A19}$$

where ρ_0 is the required ratio of the layer thicknesses; Ω_0 is the dimensionless frozen mode frequency; and K_0 is the the dimensionless wave vector associated with the frozen mode. In all numerical graphs presented in this paper we use the dimensionless notations $\omega L/c$ and kL for the frequency and the wave vector, respectively.

APPENDIX B: ANALYTIC PROPERTIES OF THE TRANSFER MATRIX $\hat{T}_L$ IN A VICINITY OF THE FROZEN MODE FREQUENCY

Consider the frequency-dependent 4×4 transfer matrix $T_L(\omega)$ in a vicinity of the frozen mode frequency ω_0,

$$\begin{aligned} &\hat{T}_L(\omega)=\hat{T}_{L0}+\nu\hat{T}_{L1}+\cdots,\ \nu=\omega-\omega_0;\\ &\hat{T}_{L0}=\hat{T}_L(\omega_0),\ \hat{T}_{L1}=\hat{T}_L'(\omega_0),\ \ldots\ . \end{aligned} \tag{B1}$$

We assume the dependence of $\hat{T}_L(\omega)$ on ω to be analytic in the vicinity of $\omega=\omega_0$. The following considerations are based on general facts from the analytic perturbation theory for the spectra of matrices.[23]

The characteristic equation (38) for $\hat{T}_L(\omega)$ has the form

$$\det[\hat{T}_L(\omega)-\zeta\hat{I}_4]=0,\quad \zeta=e^{ikL}, \tag{B2}$$

where $\hat{I}_4$ is the 4×4 identity matrix. Since $T_L(\omega)$ is a 4×4 matrix, Eq. (B2) can be recast as

$$\zeta^4+P_3(\nu)\zeta^3+P_2(\nu)\zeta^2+P_1(\nu)\zeta+1=0, \tag{B3}$$

where the complex valued functions $P_J(\nu)$, $j=0,1,2,3$ are analytic in ν in a vicinity of $\nu=0$.

According to Eq. (38), the frozen mode regime at $\nu=0$ can be ultimately characterized by the fact that for $\nu=0$ Eq. (B3) takes the following special form

$$(\zeta-\zeta_0)^3(\zeta-\zeta_1)=0,$$

where

$$\zeta_1=\zeta_0^{-3},\ |\zeta_1|=|\zeta_0|=1,\ \zeta_1\neq\zeta_0, \tag{B4}$$

where $\zeta_0=e^{ik_0L}$ corresponds to the frozen mode.

If the characteristic equation (B2) takes the special form (B4) near $\nu=0$, then $T_L(\omega)$ can be represented as follows:

$$\hat{T}_L(\omega_0+\nu)=\hat{U}(\nu)\begin{bmatrix}\zeta_1(\nu) & 0\\ 0 & \hat{Q}(\nu)\end{bmatrix}\hat{U}^{-1}(\nu), \tag{B5}$$

where $\hat{U}(\nu)$ is an invertable 4×4 matrix depending analytically on ν;

$$\zeta_1(\nu)=\zeta_1+\xi_1\nu+\xi_2\nu^2+\cdots \tag{B6}$$

is an analytic in ν complex valued function; $\hat{Q}(\nu)$ is a 3×3 matrix depending analytically on ν. In addition to that,

$$\hat{Q}(\nu)=\hat{Q}_0+\hat{Q}_1\nu+\cdots,\ \hat{Q}_0=\zeta_0\hat{I}_3+\hat{D}, \tag{B7}$$

where $\hat{I}_3$ is 3×3 identity matrix, and

$$\hat{Q}_0=\zeta_0\hat{I}_3+\hat{D} \tag{B8}$$

is the spectral decomposition (related to Jordan forms) of $\hat{Q}_0$ with $\hat{D}$ being nilpotent matrix (see Ref. 24, Sec. 6),[26] i.e.,

$$\hat{D}^3=0. \tag{B9}$$

We would like to show that Eq. (B8) is nontrivial in the sense that $\hat{D}\neq0$ and, in addition to that,

$$\hat{D}^2\neq0. \tag{B10}$$

Notice that the characteristic equation for $\hat{Q}(\nu)$ is

$$\det(\hat{Q}(\nu)-\zeta\hat{I}_3)=0,\ \zeta=e^{ikL}, \tag{B11}$$

and, in view of Eqs. (B2) and (B4) it takes the following form:

$$\begin{aligned} &(\zeta-\zeta_0)^3+[p_2\nu+O(\nu^2)](\zeta-\zeta_0)^2\\ &\quad+[p_1\nu+O(\nu^2)](\zeta-\zeta_0)+p_0\nu=0, \end{aligned} \tag{B12}$$

where

$$p_0\neq0 \tag{B13}$$

[according to Eq. (66), $p_0=6iL^3/\omega'''(k_0)$]. In view of the Caley-Hamilton theorem (see, for instance, Ref. 24, Sec. 6.2), $\hat{Q}(\nu)$ of the form (B7) satisfies the characteristic equation (B12). In other words, Eq. (B12) holds if we substitute $\zeta=\hat{Q}(\nu)$ treating all other complex numbers as scalar matrices, i.e.,

$$[\hat{Q}(\nu)-\zeta_0\hat{I}_3]^3+p_2\nu[\hat{Q}(\nu)-\zeta_0\hat{I}_3]^2+p_1\nu[\hat{Q}(\nu)-\zeta_0\hat{I}_3]+p_0\hat{I}_3\nu+O(\nu^2)=0. \tag{B14}$$

Now substituting $\hat{Q}(\nu)=\hat{Q}_0+\hat{Q}_1\nu+O(\nu^2)$ in Eq. (B14) and taking in account Eq. (B8) we single out the linear with respect to ν terms getting the following matrix equations:

$$\hat{D}^2\hat{Q}_1+\hat{D}\hat{Q}_1\hat{D}+\hat{Q}_1\hat{D}^2+p_2\hat{D}^2+p_1\hat{D}=-p_0\hat{I}_3. \tag{B15}$$

Suppose now for the sake of argument that Eq. (B10) does not hold, and hence $D^2=0$. Then Eq. (B15) turns into

$$\hat{D}\hat{Q}_1\hat{D}+p_1\hat{D}=p_0\hat{I}_3, \tag{B16}$$

implying

$$\det(\hat{D}\hat{Q}_1\hat{D}+p_1\hat{D})=\det D\det(\hat{Q}_1\hat{D}+p_1)=p_0^3. \tag{B17}$$

In view of Eq. (B9), $\det\hat{D}=0$, which together with Eq. (B17) implies that $p_0=0$, contradicting Eq. (B13). Therefore Eq. (B10) is correct and $\hat{Q}_0=\zeta_0\hat{I}_3+\hat{D}$ has nontrivial Jordan structure. In fact, in view of Eq. (B9) $\hat{Q}_0$ we have

$$\hat{Q}_0=\hat{S}_0\begin{bmatrix}\zeta_0 & 1 & 0\\ 0 & \zeta_0 & 1\\ 0 & 0 & \zeta_0\end{bmatrix}\hat{S}_0^{-1}$$

for some invertable $\hat{S}_0$. Notice also that

$$\hat{Q}(\nu)=\begin{bmatrix}0 & 1 & 0\\ 0 & 0 & 1\\ \nu & 0 & 0\end{bmatrix} \tag{B18}$$

is an exact solution to the matrix equation

$$\hat{Q}^3(\nu)=\nu I_3. \tag{B19}$$

[1] E. Yablonovich, Phys. Rev. Lett. **58**, 2059 (1987).
[2] J. Joannopoulos, R. Meade, and J. Winn, *Photonic Crystals* (Princeton University Press, Princeton, 1995).
[3] *Photonic Band Gap Materials*, edited by C. M. Soukoulis (Kluwer Academic, Dordrecht, 1996).
[4] Ph. Russell, T. Birks, and F. D. Lloyd-Lucas, *Photonic Bloch Waves and Photonic Band Gaps* (Plenum, New York, 1995).
[5] J. Rarity and C. Weisbuch, *Microcavities and Photonic Band Gaps: Physics and Applications*, Vol. 324 of *NATO Advanced Study Institute Series E: Applied Sciences* (Kluwer Academic, Dordrecht, 1996).
[6] *Special Section on Electromagnetic Crystal Structures, Design, Synthesis, and Applications*, (IEEE/OSA), 1999, Vol. 17, pp. 1925–2424.
[7] L. D. Landau, E. M. Lifshitz, and L. P. Pitaevskii, *Electrodynamics of Continuous Media* (Pergamon, New York, 1984).
[8] A. Yariv and P. Yeh, *Optical Waves in Crystals* (Wiley-Interscience, New York, 1984).
[9] A. G. Gurevich and G. A. Melkov *Magnetization Oscillations and Waves* (CRC Press, New York, 1996).
[10] A. Figotin and I. Vitebsky, Phys. Rev. E **63**, 066609 (2001).
[11] H. How and C. Vittoria, Phys. Rev. B **39**, 6823 (1989).
[12] H. How and C. Vittoria, Phys. Rev. B **39**, 6831 (1989).
[13] M. Inoue and T. Fujii, J. Appl. Phys. **81**, 5659 (1997).
[14] M. Inoue and K. Arai, J. Appl. Phys. **83**, 6768 (1998).
[15] I. Abdulhalim, J. Opt. A, Pure Appl. Opt. **2**, 557 (2000).
[16] I. Abdulhalim, J. Opt. A, Pure Appl. Opt. **1**, 646 (1999).
[17] R. Bellman, *Introduction to Matrix Analysis* (SIAM, Philadelphia, 1997).
[18] E. Coddington and R. Carlson, *Linear Ordinary Differential Equations* (SIAM, Philadelphia, 1997).
[19] B. E. A. Saleh and M. C. Teich, *Fundamentals of Photonics* (John Wiley & Sons, Inc., New York, 1991).
[20] A. Figotin, Yu. A. Godin, and I. Vitebsky, Phys. Rev. B **57**, 2841 (1998).
[21] G. D'Aguano, M. Centini, M. Scalora, *et al.*, Phys. Rev. E **64**, 016609 (2001).
[22] M. Scalora, M. J. Bloemer, *et al.*, Phys. Rev. A **56**, 3166 (1997).
[23] T. Kato, *Perturbation Theory of Linear Operators* (Springer, New York, 1995).
[24] P. Lancaster and M. Tismenetsky, *The Theory of Matrices* (Academic, New York, 1985).
[25] In the case of surface waves, the conditions for spectral asymmetry (1) are generally less stringent compared to those of the bulk waves (see, for example, Refs. 11 and 12 and references therein). Surface waves are beyond the scope of our investigation.
[26] In some publications, the matrix $\hat{\mathbf{T}}(z_2,z_1)$ from Eq. (26) is called the propagation matrix or the state matrix.